COMPUTATIONAL MODELING OF MAGNETIC FIELDS IN SOLAR ACTIVE REGIONS

TAKASHI SAKURAI

National Astronomical Observatory, Mitaka, Tokyo 181, Japan

(Received 28 July, 1988)

Abstract. The magnetic field plays an important role in various solar activities. This paper reviews techniques for computational modeling of magnetic fields in solar active regions. The input data are photospheric magnetic fields supplied by magnetograph observations. The field above the photosphere is computed by assuming an equation for the magnetic field. Three classes of magnetic fields, namely current-free fields, constant-α force-free fields, and general force-free fields are considered. Their physical/mathematical significances and computational procedures are systematically presented.

Table of Contents

Space Science Reviews **51** (1989) 11–48.

1. Introduction

1.1. Aim of this review

Various activities in the solar atmosphere originate from the magnetic field. Strong magnetic field exceeding 3000 G is found in sunspots. Areas surrounding sunspots are called plage regions and have the magnetic field of a few hundred gauss. Sunspots and plages comprise active regions (Figure 1), which literally show various activities. The most significant among them is the solar flare, an explosive conversion of magnetic energy into heat, radiation, bulk motion of gases, shock waves, and high energy particles (Švestka, 1976; Sturrock, 1980; Kundu and Woodgate, 1986). A more steady heating which is responsible for the creation of hot solar corona is also believed to be due to the presence of the magnetic field (Kuperus *et al.*, 1981). Quiet regions, which apparently show only the magnetic field of a few gauss, in actuality are composed of concentrated magnetic flux tubes (Stenflo, 1976). Active elements are, therefore, embedded everywhere in the solar atmosphere, and the active regions are places where the density of flux tubes is the largest. The magnetic activity of the Sun shows a cyclic variation whose period is about 11 years. This solar activity cycle is driven by the magnetohydrodynamic dynamo mechanism, a combined effect of rotation, convection, and the magnetic field (Cowling, 1981).

The observation of solar magnetic fields was initiated by Hale (Zirin, 1968). In the 1950's the photoelectric instruments called magnetographs were developed (Babcock, 1953) and the solar magnetic fields have been constantly monitored since then. Recent progress in instrumentation has made the observations more accurate and efficient (Hagyard, 1985).

Although the magnetic fields in prominences are observed (Leroy *et al.*, 1984), most magnetic observations give information on the photospheric magnetic field. The field in the atmosphere above is, therefore, not known observationally. The extrapolation of the magnetic field from the photosphere up into the chromosphere/corona is necessary, in order to obtain a global structure of the field. Such schemes have been extensively developed recently, relying on numerical computations. The ultimate goal we aim is to follow the evolution of the magnetic field from time to time, based on the available photospheric magnetograms. The expectation is that the solar flares manifest themselves through the change in the magnetic energy content in the atmosphere. The site of flare

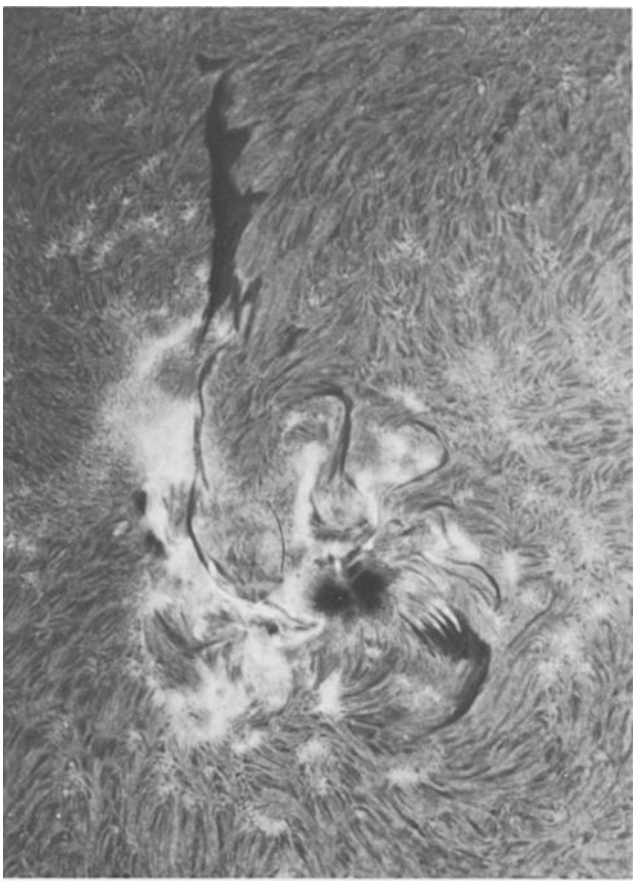

Fig. 1. The chromosphere of the Sun seen in Hα (courtesy H. Morishita, Norikura Coronagraph Station, National Astronomical Observatory of Japan).

energy release could be related to a localization of high electric current density. Hot and dense coronal plasma might be found where the magnetic field configuration is suitable for the heating mechanisms to operate. These studies require both reliable magnetic field measurements and efficient computational schemes.

On the other hand the nature of flare energy release or coronal heating will be studied more easily by isolating fundamental processes rather than looking at the full complexity of real data. Such studies, therefore, adopt simplified models (one- or two-dimensional models, for example). Let this approach be called as the idealized modeling, in contrast with the computational modeling we discussed above. These terminologies are only for convenience within this paper. The idealized modeling may sometimes be heavily computational, and the computational modeling sometimes (always?) introduces idealizing assumptions. The computational modeling in this paper means such a procedure that can produce three-dimensional magnetic field structure from the magnetic data.

In this paper we mostly concentrate on the computational modeling of magnetic fields in active region scales. Global modeling in a spherical geometry, in which the effect of the solar wind is included, was developed by Altschuler and Newkirk (1969) and has been subsequently improved (Adams and Pneuman, 1976; Altschuler *et al.*, 1977; Riesebieter and Neubauer, 1979; Levine *et al.*, 1982). For idealized modeling, see the reviews by Birn and Schindler (1981) and Low (1982).

1.2. Basic Equations

The equilibrium structure of a system of magnetic field and plasma will be described by the equation of magnetohydrostatics,

$$-\nabla p + \frac{1}{4\pi}(\mathrm{curl}\,\mathbf{B} \times \mathbf{B}) - \rho\nabla\Phi = 0\,. \tag{1.1}$$

Here p is the pressure, $\mathbf{B}$ is the magnetic field, ρ is the density, and Φ is the gravitational potential. The cgs Gaussian unit is used throughout the paper. In the chromosphere and in the corona above active regions, the effect of the magnetic field generally overwhelms the pressure and gravity forces, so that the equilibrium is approximated by

$$\mathrm{curl}\,\mathbf{B} \times \mathbf{B} = 0\,. \tag{1.2}$$

This equation defines the force-free magnetic field, in which the Lorentz force balances by itself. We may also write

$$\mathrm{curl}\,\mathbf{B} = \alpha(\mathbf{x})\mathbf{B}\,. \tag{1.3}$$

The magnetic field satisfies the divergence-free condition,

$$\mathrm{div}\,\mathbf{B} = 0\,, \tag{1.4}$$

so that Equation (1.3) leads to

$$\mathbf{B}\cdot\nabla\alpha(\mathbf{x}) = 0\,. \tag{1.5}$$

Therefore, the quantity $\alpha(\mathbf{x})$ is constant along the field line. When the value of α is the same for all the field lines, namely when α is a constant, such a class of magnetic fields is called the constant-α force-free field, namely

$$\mathrm{curl}\,\mathbf{B} = \alpha\mathbf{B}\,, \qquad \alpha = \text{constant}\,. \tag{1.6}$$

A particular case is $\alpha = 0$, which is the current-free magnetic field,

$$\mathrm{curl}\,\mathbf{B} = 0\,. \tag{1.7}$$

In this case the magnetic field can be written in terms of the scalar potential (Equation (3.5)), hence is called also as the potential field.

1.3. Coordinate System

We assume that the magnetic data are supplied in an area as large as an active region (roughly 10^5 km in size). The data are functions of X and Y, where the XY-plane is the

plane of the sky with positive X and Y toward east and north, respectively. The data are also projected onto a plane tangent to the solar (spherical) surface. This plane is designated as $z = 0$, and the magnetic field in the volume above it ($z > 0$) is to be looked for. The solution to Equation (1.2), (1.6), or (1.7) will be determined if proper boundary conditions are specified on the boundary $z = 0$.

The unit vectors $\mathbf{n}$ and $\mathbf{h}$ designate the normal (positive z) and horizontal (x and y) directions, respectively. Similarly $\mathbf{l}$ and $\mathbf{t}$ represent the unit vectors in the line-of-sight (positive Z) and transverse (X and Y) directions, respectively. The magnetic field on the plane $z = 0$ will be written as

$$\mathbf{B} = B_n\mathbf{n} + \mathbf{B}_h = B_n\mathbf{n} + B_h\mathbf{h}\,, \tag{1.8}$$

or

$$\mathbf{B} = B_l\mathbf{l} + \mathbf{B}_t = B_l\mathbf{l} + B_t\mathbf{t}\,. \tag{1.9}$$

When basic computational methods are discussed (Sections 4–6), we will restrict ourselves to the cases with $\mathbf{n} = \mathbf{l}$. General cases will be discussed only in Section 8.

The surface element $\mathrm{d}\mathbf{S}$ appears in the following sections, when converting the volume integral over $z > 0$ into the surface integral by using Gauss's theorem. The surface of integration is made of the $z = 0$ plane and a hemisphere at infinity which encloses the volume $z > 0$. On the $z = 0$ plane, $\mathrm{d}\mathbf{S}$ is given by

$$\mathrm{d}\mathbf{S} = -\mathbf{n}\,\mathrm{d}S = -\mathrm{d}x\,\mathrm{d}y\,\mathbf{n}\,. \tag{1.10}$$

1.4. Slow Evolution of Magnetic Configuration

Since the electrical conductivity of the plasma in the solar atmosphere is large enough, the plasma and the magnetic field moves together (the 'frozen-in' situation). It is advantageous to make a simplifying assumption that the plasma in the volume $z < 0$ is dense enough so that it can control the magnetic field, whereas the plasma in the volume $z > 0$ is so tenuous that the magnetic field behaves for itself. The relation between the magnetic field and the plasma motion is described by the induction equation,

$$\frac{\partial \mathbf{B}}{\partial t} = \mathrm{curl}\,(\mathbf{V} \times \mathbf{B})\,. \tag{1.11}$$

In the photosphere and below ($z < 0$), the fluid velocity $\mathbf{V}$ is determined by non-magnetic forces and Equation (1.11) describes the change in $\mathbf{B}$ responding to $\mathbf{V}$. Suppose $\mathbf{V}$ is sufficiently small so that the velocity induced in the volume $z > 0$ (the chromosphere and the corona) is negligible. Then the instantaneous state of the magnetic field in $z > 0$ is described by Equation (1.2), and a slow change in the solution reflects the change in the boundary condition. In other words we deal with the evolution of the magnetic field through a sequence of equilibria, instead of following the dynamical evolution in full.

Caution should be made that Equation (1.11) is satisfied in the volume $z > 0$ as well. The velocity $\mathbf{V}$ is small while the time scale τ is long, so that the displacement $\xi \sim O(\tau\mathbf{V})$ is finite. This leads to a finite change in the magnetic field. Equation (1.1) or (1.2) only assumes that $\mathbf{V}$ is negligible, which does not mean that $\mathbf{V} = 0$.

In Section 2 we briefly review the observation of magnetic fields. In Section 3 fundamental properties of the magnetic field are summarized. In Sections 4 to 6, we discuss the modeling in the progressive order of complexity, namely, the current-free field (Section 4), the constant-α force-free field (Section 5), and the force-free field in general (Section 6). Section 7 presents the applications of various techniques discussed in this paper.

2. Observation of Magnetic Fields

Magnetic fields in the solar atmosphere are constantly monitored by an instrument called the magnetograph. In the presence of the magnetic field, the light coming from the solar atmosphere is polarized due to the Zeeman effect. The magnetograph measures this polarization and derives information on the solar magnetic fields. This section outlines fundamental processes for the measurement of solar magnetic fields. For more details, see e.g. Stenflo (1971, 1976).

2.1. Stokes parameters

The polarization of light is described in terms of the so-called Stokes parameters (Chandrasekhar, 1960a). Suppose the light propagating in the z-direction has an electric vector

$$E_x = E_1 \cos(\omega t - \phi_1), \tag{2.1}$$

$$E_y = E_2 \cos(\omega t - \phi_2). \tag{2.2}$$

Denoting the time average by $\overline{\ }$, we introduce

$$I_1 = \overline{E_1^2}, \qquad I_2 = \overline{E_2^2}. \tag{2.3}$$

Then the Stokes parameters I, Q, U, and V are defined as

$$I = I_1 + I_2, \tag{2.4}$$

$$Q = I_1 - I_2, \tag{2.5}$$

$$U = \overline{2E_1E_2 \cos(\phi_1 - \phi_2)}, \tag{2.6}$$

and

$$V = \overline{2E_1E_2 \sin(\phi_1 - \phi_2)}. \tag{2.7}$$

The Stokes Q and U represent the linear polarization, and V corresponds to the circular polarization. Positive V is for right-hand circular polarization viewed from the observer (i.e., from the positive z-direction) in our definition. The Stokes I is the total intensity and satisfies the relation

$$I^2 \geqq Q^2 + U^2 + V^2. \tag{2.8}$$

The equality holds if the light is perfectly polarized. Figure 2 shows some representative cases.

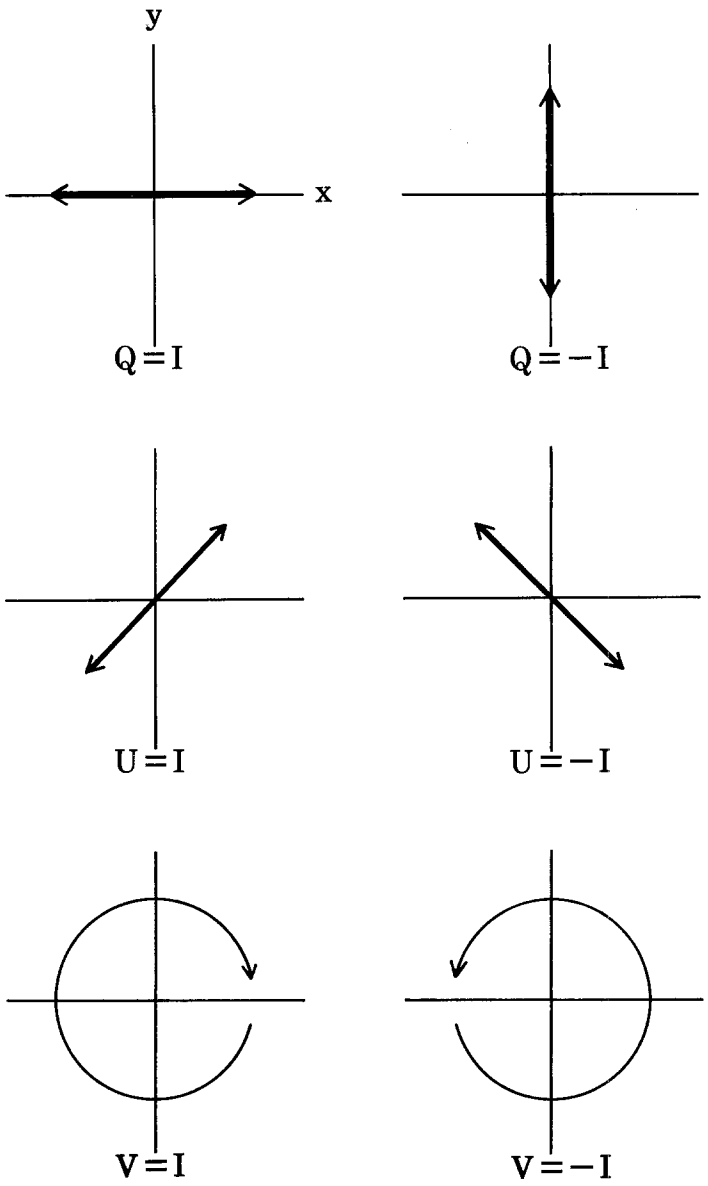

Fig. 2. Stokes parameters Q, U, and V for perfectly polarized light. Arrows represent the trajectories of the electric field vector as viewed from the observer.

2.2. Zeeman effect of spectral lines

The absorption of light by an atom placed in the magnetic field (the Zeeman effect) is described as follows (Bray and Loughhead, 1979). In the classical theory of radiation, an atom is represented by a dipole oscillator. Suppose an electron in an atom oscillates with the frequency ν_0. This atom absorbs the light near this frequency. When this atom is placed in the magnetic field, the motion of the electron along the magnetic field is not

affected. In the plane perpendicular to the magnetic field, however, the electron now undergoes the precession which is counterclockwise as viewed from the direction of the magnetic field. The frequency of the precession is the Larmor frequency

$$\Delta\nu_H = \frac{eg_L H}{4\pi m_e c} = 1.40 \times 10^6 g_L H \quad \text{(Hz)}, \tag{2.9}$$

where m_e and $-e$ are electronic mass and charge respectively, c is the speed of light, g_L is the Landé factor, and H is the magnetic field strength in gauss. The motion of the precessing oscillator is the superposition of two oppositely directed circular motions: the counterclockwise (left-hand circular) motion with the frequency $\nu_0 + \Delta\nu_H$, and the clockwise (right-hand circular) motion with the frequency $\nu_0 - \Delta\nu_H$. These two components are called σ-components. In the wavelength domain, they appear at $\lambda_0 - \Delta\lambda_H$ and $\lambda_0 + \Delta\lambda_H$, respectively. Here $\lambda_0 = c/\nu_0$ and

$$\Delta\lambda_H = \lambda_0^2 \Delta\nu_H / c = 11.7 g_L \frac{H}{1000\ \text{G}} \left(\frac{\lambda}{5000\ \text{Å}}\right)^2 \quad \text{(mÅ)}. \tag{2.10}$$

When we observe the atom from the direction of the magnetic field, the former component, which appears at the shorter wavelength, absorbs the left-hand circularly polarized light selectively. The original unpolarized light therefore becomes right-hand circularly polarized after passing through the gas. The opposite situation takes place for the longer wavelength component (Figure 3(a)).

On the other hand when we look at the atom from the direction perpendicular to the magnetic field, σ-components absorb the light whose electric vector is in the plane perpendicular to the magnetic field. The other component (π-component) absorbs the light polarized along the magnetic field. Therefore, after passing through the gas, the unpolarized light becomes linearly polarized. The direction of polarization of the σ-components is along the magnetic field (Figure 3(b)).

2.3. Transfer of Polarized Light

The final state of the polarization of light after passing through the solar atmosphere will be obtained by solving the equation of radiative transfer (Landi Degl'Innocenti, 1976). Let

$$\mathbf{I}(\tau) = (I(\tau), Q(\tau), U(\tau), V(\tau)), \tag{2.11}$$

$$\mathbf{S}(\tau) = (S(\tau), 0, 0, 0), \tag{2.12}$$

where τ is the continuum optical depth and $S(\tau)$ is the source function. Then the equation of radiative transfer is

$$\mu \frac{d\mathbf{I}}{d\tau} = (\mathbf{1} + \eta_0 A)(\mathbf{I} - \mathbf{S}). \tag{2.13}$$

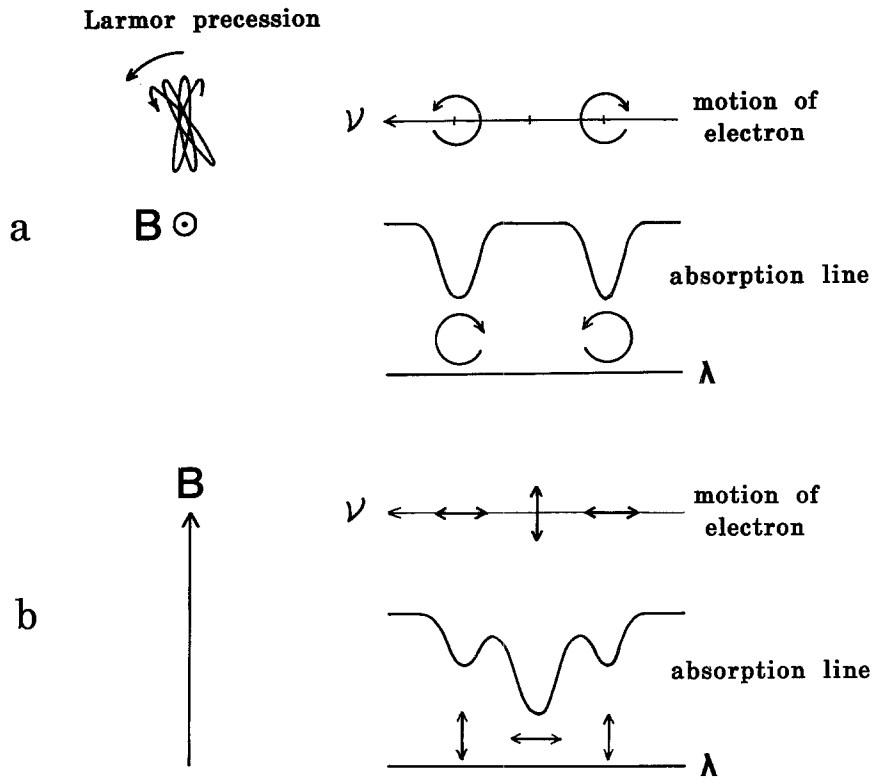

Fig. 3. Longitudinal (a) and transverse (b) Zeeman effects. In the longitudinal case, te absorption line is split into two σ-components which are circularly polarized in the opposite sense with each other. In the transverse case, the central π-component and the two σ-components are linearly polarized in the direction orthogonal to each other. The direction of the polarization of the σ-components is along the magnetic field vector.

Here **1** denotes the unit matrix, and $\mu = \cos\theta$ where θ is the angle between the line-of-sight and the solar surface normal. Further, η_0 is defined as

$$\frac{\kappa(\text{line})}{\kappa(\text{continuum})} = \eta_0 H(a, v)\,, \tag{2.14}$$

where κ stands for the absorption coefficient, H is the Voigt function, a is the damping constant, and

$$v = (\lambda - \lambda_0)/\Delta\lambda_D\,, \tag{2.15}$$

with the Doppler with $\Delta\lambda_D$. The matrix A is given by

$$A = \begin{bmatrix} \eta_I & \eta_Q & 0 & \eta_V \\ \eta_Q & \eta_I & \rho_V & 0 \\ 0 & -\rho_V & \eta_I & \rho_Q \\ \eta_V & 0 & -\rho_Q & \eta_I \end{bmatrix}. \tag{2.16}$$

This expression for A assumes that the magnetic field has a constant direction and $+Q$ axis is along the field. The so-called magneto-optical effect appears through ρ's, which will be discussed later. Here we neglect this effect and set $\rho = 0$, so that $U = 0$ holds. The remaining quantities are defined as

$$\eta_I = \tfrac{1}{2}[H(a, v) \sin^2 \psi + \tfrac{1}{2}\{H(a, v - v_H) + H(a, v + v_H)\} (1 + \cos^2 \psi)] , \tag{2.17}$$

$$\eta_Q = \tfrac{1}{2}[H(a, v) - \tfrac{1}{2}\{H(a, v - v_H) + H(a, v + v_H)\} \sin^2 \psi] , \tag{2.18}$$

$$\eta_V = \tfrac{1}{2}[H(a, v - v_H) - H(a, v + v_H)] \cos \psi , \tag{2.19}$$

where ψ is the angle between the magnetic field and the line-of-sight, and

$$v_H = \Delta\lambda_H / \Delta\lambda_D . \tag{2.20}$$

Hereafter we assume that the parameters a, v_H, and ψ are constants, independent of τ. Unno (1956) obtained the solution to this problem when η_0 is a constant. Makita (1979) extended the solution to an arbitrary form for $\eta_0(\tau)$. The state of polarization at $\tau = 0$ which we observe is written as

$$I = \tfrac{1}{2}(W_+ + W_-) , \tag{2.21}$$

$$\frac{V}{\eta_V} = \frac{Q}{\eta_Q} = \frac{1}{2\sqrt{\eta_Q^2 + \eta_V^2}} (W_+ - W_-) , \tag{2.22}$$

where

$$W_\pm = \int_0^\infty \frac{B(\tau)}{\mu} (1 + \eta_0 \eta_\pm) \exp[-(\tau + \eta_\pm \zeta)/\mu] , \tag{2.23}$$

$$\eta_\pm = \eta_0 \pm \sqrt{\eta_Q^2 + \eta_V^2} , \tag{2.24}$$

$$\zeta = \int \eta_0(\tau) \, \mathrm{d}\tau . \tag{2.25}$$

2.4. Determination of magnetic fields

If the magnetic field is weak so that $\Delta\lambda_H \ll \Delta\lambda_D$, we can expand the above expressions in terms of v_H. In this weak field approximation, we obtain

$$V = -v_H \cos \psi \frac{\mathrm{d}I}{\mathrm{d}v} , \tag{2.26}$$

and

$$Q = -\frac{v_H^2}{4} \sin^2 \psi \frac{H''}{H'} \frac{\mathrm{d}I}{\mathrm{d}v} , \tag{2.27}$$

where prime (′) denotes differentiation with respect to v_H. If the transverse magnetic field makes the angle χ with respect to the $+Q$ axis, Equation (2.27) is replaced with

$$Q = -\frac{v_H^2}{4}\sin^2\psi\frac{H''}{H'}\frac{\mathrm{d}I}{\mathrm{d}v}\cos 2\chi\,, \tag{2.28}$$

$$U = -\frac{v_H^2}{4}\sin^2\psi\frac{H''}{H'}\frac{\mathrm{d}I}{\mathrm{d}v}\sin 2\chi\,. \tag{2.29}$$

Therefore, the circular polarization degree is proportional to the line-of-sight component (B_l) of the magnetic field, whereas the linear polarization is proportional to the square of the transverse component (B_t) of the magnetic field. Namely,

$$V \sim B_l\,, \tag{2.30}$$

$$Q \sim B_t^2\cos 2\chi = B_X^2 - B_Y^2\,, \tag{2.31}$$

$$U \sim B_t^2\sin 2\chi = 2B_XB_Y\,. \tag{2.32}$$

The azimuth of the linear polarization is along the direction of the transverse magnetic field, either in parallel or antiparallel. This ambiguity is always associated with the polarization measurement, and can be resolved by introducing additional assumptions (see Section 7). If the weak field approximation is not valid, the conversion from the polarization to the field strength is more involved.

The instruments which can record the profiles of Stokes parameters are called the Stokes polarimeters. Usual magnetographs only measure the Stokes parameters integrated over a narrow band of wavelength in the wing of a spectral line. Vector magnetographs measure both the circular and linear polarizations, whereas usual (longitudinal) magnetographs only record the circular polarization. Currently achieved accuracy in the measurement is a factor times 10^{-4} in the polarization degree, which amounts to a few gauss in the longitudinal field and a few tens of gauss in the transverse field, respectively.

2.5. Applicability of Assumptions

The measurement of polarization is a very delicate task and requires extreme care. In addition we had to introduce many assumptions above, in order to extract the information on the solar magnetic field from the polarization measurement. We will now discuss the validity of these assumptions briefly.

(a) *Magneto-Optical Effect*

Generally the absorption of light by the atom, represented by the imaginary part of the index of refraction, comes together with the retardation effect. The variation of the real part of the index of refraction (n) in the absence of the magnetic field is like

$$n - 1 \sim v/(v^2 + a^2)\,. \tag{2.33}$$

Therefore, the phase of light advances or delays in the wings of the spectral line. In the presence of the magnetic field, the retardation is caused by all the three Zeeman components. Let us consider the linearly polarized light propagating in the direction of the magnetic field. The consequence is that the direction of the polarization rotates clockwise in the wing and counter-clockwise near the center of the line, as viewed from the direction of the field. This is the well-known Faraday rotation. This effect is certainly present near sunspots where the field strength exceeds 1000 G (Landi Degl'Innocenti, 1979; Kawakami, 1983; West and Hagyard, 1983).

(b) *Flux Tubes and Canopy Structure*

We have so far assumed that the magnetic field we measure is uniform within the aperture of the magnetograph as well as in the line-forming layer in the solar atmosphere. If the weak field approximation is valid, we can deduce the longitudinal field strength from the circular polarization degree.

When the field is not uniform, we can still deduce the average longitudinal field (or the magnetic flux) within the aperture, provided (i) the weak field approximation is valid, and (ii) the profile of the spectral line does not change within the aperture. Under such circumstances we have

$$\langle V \rangle \sim \langle B_l \rangle \,, \tag{2.34}$$

where the brackets $\langle\ \rangle$ represent spatial averaging.

For the transverse field, the situation is more involved. We write

$$\mathbf{B}_t = \langle \mathbf{B}_t \rangle + \delta \mathbf{B}_t \,, \qquad \langle \delta \mathbf{B}_t \rangle = 0 \,. \tag{2.35}$$

Then from Equations (2.31) and (2.32) we obtain

$$\langle Q \rangle \sim \langle B_X \rangle^2 - \langle B_Y \rangle^2 \,, \qquad \langle U \rangle \sim 2 \langle B_X \rangle \langle B_Y \rangle \,, \tag{2.36}$$

provided

$$\langle \delta B_X^2 \rangle = \langle \delta B_Y^2 \rangle \,, \qquad \langle \delta B_X \delta B_Y \rangle = 0 \,. \tag{2.37}$$

That is, the observation gives the average transverse vector. On the other hand if the transverse magnetic field is inhomogeneous but uni-directional (e.g., $\delta B_Y = 0$, $\langle \delta B_X^2 \rangle \neq 0$), the observation gives the root-mean-square transverse field strength (Beckers, 1971).

However, we have now good reason to believe that both presumptions (i) and (ii) are violated. Weak magnetic field on the Sun is not really weak, and is composed of elementary flux tubes which occupy only a small fraction of the solar surface (Stenflo, 1976; Harvey, 1977). Magnetic fields are concentrated into the flux tubes whose size is only 100–200 km and the field strength there is as high as 1000 G, due to the interaction between the magnetic field and the convective flow (Parker, 1979, Chapter 10). Therefore the weak field approximation will not apply. Further, the excess magnetic heating in the flux tubes makes the absorption lines there shallower than in the surrounding non-magnetic atmosphere. Due to these effects, the signal from the magnetograph does not give the correct average magnetic field.

Magnetic field lines fan out from the flux tubes and merge together to make a larger scale structure. In between the flux tubes the field lines are nearly horizontal, overlying the non-magnetic atmosphere. This canopy structure (Giovanelli, 1980) also complicates the interpretation of the polarization measurement, especially the derivation of the transverse magnetic field.

From the argument given above, the observation of the solar magnetic field requires not only the accurate polarization measurement but also the understanding of the nature of the solar magnetic field. In the following sections we shift our attention to the modeling of the magnetic field. However, we should keep in mind that the available data are subject to many uncertainties.

3. General Properties of Magnetic Fields

3.1. Representation of Magnetic Fields

From the divergence-free condition for the magnetic field, Equation (1.4), we can write

$$\mathbf{B} = \operatorname{curl} \mathbf{A}\,, \tag{3.1}$$

where $\mathbf{A}$ is the vector potential. Since the gradient of any scalar can be added to $\mathbf{A}$ without altering $\mathbf{B}$, the vector potential is not unique. This freedom in $\mathbf{A}$ is restricted in one way by imposing the so-called gauge condition. The other way is to adopt the toroidal/poloidal decomposition (Morse and Feshbach, 1953)

$$\mathbf{A} = T\mathbf{a} + \operatorname{curl}(P\mathbf{a})\,, \tag{3.2}$$

where T and P are called toroidal and poloidal scalars. The vector $\mathbf{a}$ may either be $\mathbf{a} = \hat{\mathbf{z}}$ (the unit z-vector) or $\mathbf{a} = \mathbf{x}$ (the position vector).

Another representation for $\mathbf{B}$ is via Euler potentials (Stern, 1966),

$$\mathbf{B} = \nabla f \times \nabla g\,. \tag{3.3}$$

Since $\mathbf{B} \cdot \nabla f = \mathbf{B} \cdot \nabla g = 0$, the Euler potentials f and g are constant along the field line. In other words, a pair of f and g labels the field line. This representation is always possible locally, but regular and single-valued functions f and g may not exist globally. The potentials (f, g) can be changed to (f', g') without altering $\mathbf{B}$ if

$$\frac{\partial(f', g')}{\partial(f, g)} = 1\,. \tag{3.4}$$

When the magnetic field $\mathbf{B}$ is curl-free (current-free), one can introduce a scalar potential ϕ,

$$\mathbf{B} = -\nabla\phi\,, \tag{3.5}$$

and $\operatorname{div}\mathbf{B} = 0$ requires that ϕ satisfies the Laplace equation,

$$\Delta\phi = 0\,. \tag{3.6}$$

Note that Equations (3.1) and (3.3) are based on the divergence-free condition (1.4) which is always satisfied by **B**. Equation (3.5), however, only applies to the current-free magnetic field, and is meaningful only when the Laplace equation (3.6) is satisfied.

3.2. Conservation laws

The magnetic field satisfies various conservation laws. The conservation of magnetic flux is the most fundamental one. We will discuss other conservation laws which are derived from the frozen-in condition.

(a) *Advection of Euler Potentials*

We can show that if the Euler potentials (f, g) evolve acording to

$$\frac{\mathrm{d}f}{\mathrm{d}t} = \frac{\mathrm{d}g}{\mathrm{d}t} = 0 \qquad \left(\frac{\mathrm{d}}{\mathrm{d}t} = \frac{\partial}{\partial t} + \mathbf{V}\cdot\nabla\right), \tag{3.7}$$

then the induction equation (1.11) is satisfied. This is natural because the pair of (f, g) labels the field line which moves with the fluid. Equation (3.7) is sufficient but not necessary for the frozen-in condition to be satisfied. We can re-label the field lines within the restriction of Equation (3.4).

(b) *Magnetic Helicity*

The magnetic helicity is defined by

$$H = \int \mathbf{A}\cdot\mathbf{B}\,\mathrm{d}V. \tag{3.8}$$

By changing $\mathbf{A}$ to $\mathbf{A}' = \mathbf{A} + \nabla G$, we obtain

$$H' = \int \mathbf{A}'\cdot\mathbf{B}\,\mathrm{d}V = H + \int G\mathbf{B}\cdot\mathrm{d}\mathbf{S}. \tag{3.9}$$

We can see that H is not invariant against the change in the gauge of $\mathbf{A}$ when the magnetic field lines cross the boundary of the integration volume. Suppose a special case that the medium in the volume $z \leqq 0$ is at rest. Then we may fix the gauge in $z \leqq 0$ such that $G = 0$, and $G(z > 0)$ does not affect the value of H. (A more rigorous procedure was taken by Berger and Field (1984), who introduced a gauge-invariant generalization of the helicity.)

From the induction equation (1.11) the vector potential is found to satisfy

$$\frac{\partial\mathbf{A}}{\partial t} = \mathbf{V}\times\mathbf{B} + \nabla\Psi, \tag{3.10}$$

where Ψ is an arbitrary scalar function. We can then show that

$$\frac{\mathrm{d}H}{\mathrm{d}t} = \int (\Psi + \mathbf{V}\cdot\mathbf{A})\mathbf{B}\cdot\mathrm{d}\mathbf{S}. \tag{3.11}$$

Therefore, the helicity H is conserved when the field lines are closed within the volume of interest ($\mathbf{B} \cdot \mathrm{d}\mathbf{S} = 0$). Similarly when the external medium ($z \leqq 0$) is at rest, we can set $\Psi = 0$ and $\mathbf{V} = 0$ on the boundary, and the helicity is conserved.

(c) *Energy Conservation*

The magnetic energy W is defined by

$$W = \int \frac{B^2}{8\pi} \mathrm{d}V . \tag{3.12}$$

The rate of change in W is, therefore,

$$\frac{\mathrm{d}W}{\mathrm{d}t} = -\int \frac{1}{c}(\mathbf{j} \times \mathbf{B}) \cdot \mathbf{V} \, \mathrm{d}V + \int \left[\frac{1}{4\pi}(\mathbf{V} + \mathbf{B}) \times \mathbf{B} + \frac{B^2}{8\pi}\mathbf{V} \right] \cdot \mathrm{d}\mathbf{S} . \tag{3.13}$$

The first term is the work done by the Lorentz force, and the second term is the Poynting influx through the boundary. The third term is due to the change in the volume considered, and can be dropped in our present situation.

3.3. Global Force Balance and Virial Relations

By integrating Equation (1.2) over the volume, we obtain the equations for the global force balance (Molodensky, 1969, 1974; Low, 1985),

$$F_x = -\frac{1}{4\pi} \int B_x B_z \, \mathrm{d}x \, \mathrm{d}y = 0 , \tag{3.14}$$

$$F_y = -\frac{1}{4\pi} \int B_y B_z \, \mathrm{d}x \, \mathrm{d}y = 0 , \tag{3.15}$$

$$F_z = \frac{1}{4\pi} \int (B_x^2 + B_y^2 - B_z^2) \, \mathrm{d}x \, \mathrm{d}y = 0 . \tag{3.16}$$

If these F's are non-zero, it means the existence of non-magnetic forces counter-acting against the net magnetic force (F_x, F_y, F_z) (Figure 4).

Similarly the overall torque must vanish, namely,

$$T_x = \frac{1}{4\pi} \int y(B_x^2 + B_y^2 - B_z^2) \, \mathrm{d}x \, \mathrm{d}y = 0 , \tag{3.17}$$

$$T_y = -\frac{1}{4\pi} \int x(B_x^2 + B_y^2 - B_z^2) \, \mathrm{d}x \, \mathrm{d}y = 0 , \tag{3.18}$$

$$T_z = -\frac{1}{4\pi} \int (yB_x B_z - xB_y B_z) \, \mathrm{d}x \, \mathrm{d}y = 0 . \tag{3.19}$$

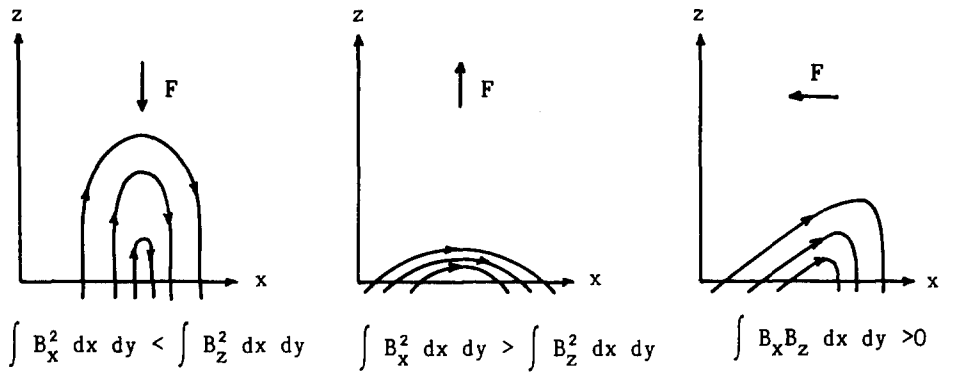

Fig. 4. Net magnetic force **F** derived from the global force balance equations (3.14)–(3.16) (Sakurai, 1987).

By taking the dot product of Equation (1.2) with **x**, we obtain,

$$W = \frac{1}{4\pi}\int (xB_x + yB_y)B_z\,dx\,dy\,. \tag{3.20}$$

The last four equations are a part of tensor virial relations (Chandrasekhar, 1960b). Although the coordinate **x** appears explicitly in Equations (3.17)–(3.20), the selection of the origin of **x** does not affect these equations because of Equations (3.14)–(3.16). Of particular importance is Equation (3.20), which gives the magnetic energy content in terms of the boundary values of **B**.

3.4. Topological Properties of Magnetic Fields

(a) *Connectivity of Field Lines*

Field lines connect two points, the starting and the end points. The correspondence (mapping) between the two points is the connectivity of the field line. The connectivity is most easily specified by the distribution of the Euler potentials (f, g) on the boundary (Antiochos, 1987). When more than two points share the same value of (f, g), an additional condition is necessary to uniquely determine the connectivity. Usually the evolutional constraint is imposed in such a case, in that the connectivity should be the same as the initial state.

(b) *Helicity*

The magnetic helicity defined by Equation (3.8) is a measure of how the system of field lines are twisted (Berger and Field, 1984). As an example, let us consider two isolated flux rings which themselves are not twisted and whose magnetic fluxes are Φ_1 and Φ_2, respectively. The helicity of this system is $H = 0$ if the two rings are disconnected, while $H = \pm 2\Phi_1\Phi_2$ if the rings are connected like a chain.

(c) *Number of Neutral Points*

Molodensky and Syrovatsky (1977) considered the Poincaré index of magnetic fields. Near the magnetic neutral point $\mathbf{x}_0$, the magnetic field is approximated by

$$\mathbf{B} = D(\mathbf{x} - \mathbf{x}_0)\,, \tag{3.21}$$

where D is a constant matrix. The Poincaré index is defined as the sum of the signs of $\det(D)$ over the volume.

First we will consider the projection of magnetic field lines on the $z = 0$ plane. Sources or sinks of field lines like sunspots have the Poincaré index of $+1$, whereas magnetic neutral points (saddle points) have the index of -1 (Figure 5, 2-D). Suppose the magnetic flux in the region considered is balanced, and the net dipole moment is non-zero. Then this region is regarded as a dipole when seen from large distances, and its Poincaré index is 2. Therefore,

$$M_+ + M_- - C = 2\,, \tag{3.22}$$

where $M_\pm$ is the number of sources/sinks, and C is the number of saddle points.

Next we will consider the three-dimensional configuration. The volume $z < 0$ is assumed as the mirror reflection of $z > 0$. Sources or sinks only exist on the plane $z = 0$. Saddles may exist in the volume $z > 0$, but they always make a pair with the saddles with the opposite signs of $\det(D)$ in $z < 0$, so that only the saddles on the plane $z = 0$ contribute to the Poincaré index of the system. Since the three-dimensional Poincaré index (Figure 5, 3-D) of the dipole is 0, we obtain

$$M_+ - M_- - C_+ + C_- = 0\,, \tag{3.23}$$

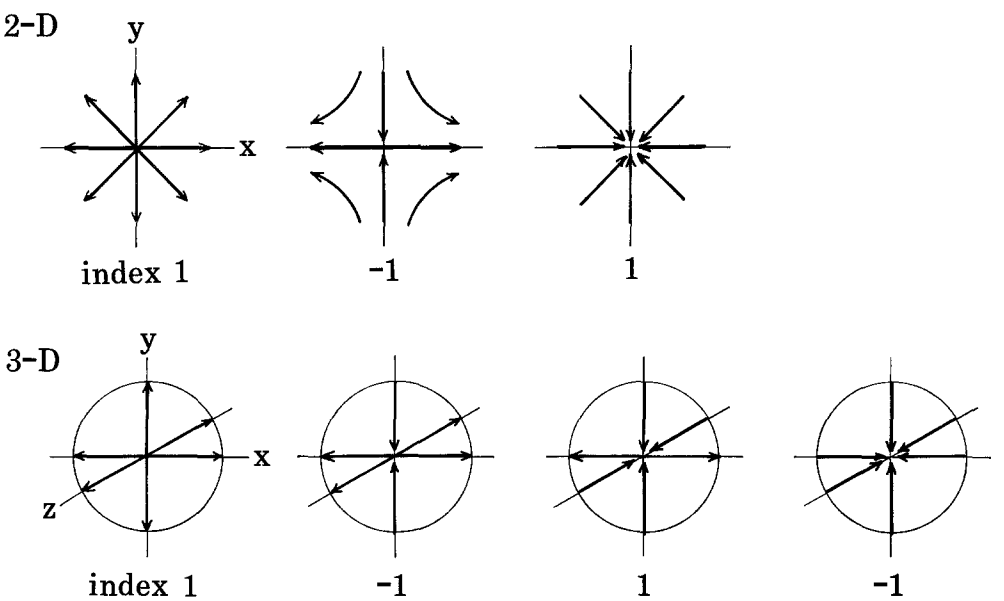

Fig. 5. Poincaré indices of magnetic neutral points in the two- and three-dimensional cases.

where $C_+ + C_- = C$. From Equations (3.22) and (3.23) we find

$$C_+ = M_+ - 1\,, \qquad C_- = M_- - 1\,. \tag{3.24}$$

The Poincaré index of the volume $z > z_0$ can be calculated by the formula

$$N(z_0) = \int \frac{1}{4\pi B^3} \begin{vmatrix} 0 & B_x & B_y & B_z \\ \mathrm{dS} & \nabla B_x & \nabla B_y & \nabla B_z \end{vmatrix}\,. \tag{3.25}$$

Here the integration is to be carried out over the plane $z = z_0$ and a semi-spherical surface extending to $z = \infty$. Note that the contribution from the latter surface does not vanish, so that this equation is of little use practically.

4. Current-Free Magnetic Fields

Because of computational tractability, current-free modeling has been carried out in numerous applications. Although the current-free approximation is the most crude among the three classes treated in this paper, we should not overlook the usefulness of the current-free modeling. This model will give us a general idea of the three-dimensional magnetic field configuration, which we cannot observe directly. The deviation of current-free field lines from the observed magnetic structures (tracers) suggests the degree of distortion in the magnetic field.

4.1. Boundary Value Problem

We will adopt the expression for **B** in terms of the scalar potential (3.5). The equation to be solved is Equation (3.6), and when a proper boundary condition is supplied, the solution exists and is unique. In the Dirichlet problem, the value of the potential ϕ is specified on the boundary. In the Neumann problem, the normal derivative of the potential is given as the boundary condition. The latter fits into our situation because $B_n = -\partial\phi/\partial n$ is the observed quantity. The boundary value problem now is to find $\mathbf{B} = -\nabla\phi$ such that

$$\Delta\phi = 0\ (z > 0)\,, \qquad -\mathbf{n}\cdot\nabla\phi = B_n\ (z = 0)\,. \tag{4.1}$$

We also require that the field strength decays to zero at infinity.

4.2. Variational Principle

The variational principle in this case is well known as Thompson's principle. If the scalar potential representation (3.5) is used, the variational principle for the energy W given by Equation (3.12) corresponds to the Dirichlet boundary value problem. In order to obtain the Neumann problem, we have to modify W into W',

$$W' = \int \frac{(\nabla\Phi)^2}{8\pi}\,\mathrm{d}V + \int B_n\phi\,\mathrm{d}S\,. \tag{4.2}$$

The variation of W' yields

$$4\pi\delta W' = -\int \Delta\phi\,\delta\phi\,\mathrm{d}V + \int \left(\frac{\partial\phi}{\partial n} + B_n\right)\delta\phi\,\mathrm{d}S\,. \tag{4.3}$$

Namely, the extremum satisfies the Laplace equation when the Neumann boundary condition is specified. The extremum is actually the absolute minimum. Therefore the current-free field, being the minimum energy state, is free from any instabilities.

The variation of energy W when the vector potential representation (3.1) is adopted is

$$4\pi\delta W = \int \delta\mathbf{A}\cdot\operatorname{curl}\mathbf{B}\,\mathrm{d}V + \int \mathbf{B}\cdot(\mathrm{d}\mathbf{S}\times\delta\mathbf{A})\,. \tag{4.4}$$

When $\mathrm{d}\mathbf{S}\times\mathbf{A}$ is specified on the boundary, the energy W is stationary if $\mathbf{B}$ is curl-free. To give $\mathrm{d}\mathbf{S}\times\mathbf{A}$ is equivalent to give B_n.

There are two kinds of computational methods for the current-free field, namely the Green's function method and the Fourier expansion. We will discuss each of them in the following.

4.3. Green's function method

In the Green's function method, the solution to Equation (4.1) is written as

$$\phi(\mathbf{x}) = \int B_n(\mathbf{x}')G_n(\mathbf{x},\mathbf{x}')\,\mathrm{d}x'\,\mathrm{d}y'\,. \tag{4.5}$$

The expression for the Green's function G_n is

$$G_n(\mathbf{x},\mathbf{x}') = \frac{2\pi}{|\mathbf{x}-\mathbf{x}'|}\,. \tag{4.6}$$

This formula was first applied to the solar magnetic field by Schmidt (1964). It is easy to confirm that Equation (4.1) solves the problem, since G_n satisfies the Laplace equation and $-\partial G_n/\partial z$ becomes the delta function as $z\to 0$. G_n represents the potential of a monopole whose magnetic flux in $z>0$ is unity.

4.4 Fourier expansion method

In the Fourier expansion method (Teuber *et al.*, 1977), ϕ is written as

$$\phi = \sum_{\mathbf{k}_\perp} \phi_{\mathbf{k}_\perp} \exp(i\mathbf{k}_\perp\cdot\mathbf{x}_\perp - k_\perp z)\,, \tag{4.7}$$

where $\mathbf{k}_\perp = (k_x, k_y)$, $k_\perp = \sqrt{k_x^2 + k_y^2}$, and $\mathbf{x}_\perp = (x, y)$. The Laplace equation (3.6) is then satisfied. The boundary value B_n is also expanded as

$$B_n = \sum_{\mathbf{k}_\perp} B_{\mathbf{k}_\perp} \exp(i\mathbf{k}_\perp\cdot\mathbf{x}_\perp) + B_{n0}\,, \tag{4.8}$$

where B_{n0} is a constant, and the summation $\sum$ excludes $\mathbf{k}_\perp = 0$. The relation between

$B_{\mathbf{k}_\perp}$ and $\phi_{\mathbf{k}_\perp}$ is found as

$$\phi_{\mathbf{k}_\perp} = B_{\mathbf{k}_\perp}/k_\perp \quad (\mathbf{k}_\perp \neq 0)\,. \tag{4.9}$$

The three components of the field are

$$B_x = -\sum_{\mathbf{k}_\perp} i(k_x/k_\perp)B_{\mathbf{k}_\perp} \exp(i\mathbf{k}_\perp \cdot \mathbf{x}_\perp - k_\perp z)\,, \tag{4.10}$$

$$B_y = -\sum_{\mathbf{k}_\perp} i(k_y/k_\perp)B_{\mathbf{k}_\perp} \exp(i\mathbf{k}_\perp \cdot \mathbf{x}_\perp - k_\perp z)\,, \tag{4.11}$$

$$B_z = B_{n0} + \sum_{\mathbf{k}_\perp} B_{\mathbf{k}_\perp} \exp(i\mathbf{k}_\perp \cdot \mathbf{x}_\perp - k_\perp z)\,. \tag{4.12}$$

The DC component B_{n0} represents the imbalance in the magnetic flux within the domain of consideration, and should be made negligible by properly selecting the area of computation.

5. Constant-α Force-Free Fields

5.1. Variational Principle

In the case of the current-free field, the minimizing solution is sought for among the family of trial functions which are only constrained to possess the same flux distribution on the boundary. If an additional constraint is imposed on the trial functions so that the area for searching the energy minimum is restricted, we would find a different energy minimum. The more strict the constraint is, the narrower the area of minimum search and consequently the larger the value of minimum energy.

Woltjer (1958, 1959) considered the extremum of W when the helicity H is held fixed. By introducing the Lagrangian multiplier α, the quantity to be made stationary is

$$W'' = \frac{1}{8\pi}\int \{(\mathrm{curl}\,\mathbf{A})^2 - \alpha \mathbf{A}\cdot\mathrm{curl}\,\mathbf{A}\}\,\mathrm{d}V\,. \tag{5.1}$$

The variation of W'' is

$$4\pi\delta W'' = \int \delta\mathbf{A}\cdot(\mathrm{curl}\,\mathbf{B} - \alpha\mathbf{B})\,\mathrm{d}V + \int \left(\mathbf{B} - \frac{\alpha\mathbf{A}}{2}\right)\cdot(\mathrm{d}\mathbf{S}\times\delta\mathbf{A})\,. \tag{5.2}$$

Here $\mathrm{d}\mathbf{S}\times\mathbf{A}$ is held fixed on the boundary (i.e., B_n is fixed). Therefore, the extremum takes place for the constant-α force-free field, Equation (1.6).

Whether the extremum is minimum or not depends on the magnitude of α. As long as α is small, the constant-α fields will have the same property as the current-free field and will take the minimum energy (Molodensky, 1975). At the instant when the minimum turns into a saddle point, the energy contour in a magnetic 'phase space' will be very flat. This situation corresponds to the appearance of multiple solutions. As is described below, the constant-α solution takes the minimum energy if $|\alpha|$ is smaller than the smallest eigenvalue of Equation (5.5) (Berger, 1985).

5.2. Boundary value problem

By adopting the toroidal/poloidal decomposition for **B** (Equation (3.2)) with $\mathbf{a} = \hat{\mathbf{z}}$, Equation (1.6) leads to

$$T = \alpha P, \qquad (\Delta + \alpha^2)P = 0. \tag{5.3}$$

Therefore, the equation to be solved is the Helmholtz wave equation. This observation immediately implies some difficulties associated with the constant-α force-free field. The boundary condition imposed by the observation is

$$B_n = -\left(\frac{\partial^2}{\partial x^2} + \frac{\partial^2}{\partial y^2}\right)P \quad (z = 0). \tag{5.4}$$

The boundary condition at infinity is a problem. In the case of the current-free field, solutions at infinity either diverge or decay to zero. Therefore, we impose the boundary condition in order to select the solution that decays to zero. All the solutions to Equation (5.3) however decay like $P \sim \exp(\pm i\alpha r)/r$ $(r \to \infty)$. The selection of $\pm$ signs can be made by the so-called radiation condition when studying the waves by Equation (5.3). In our case no such conditions are appropriate. We do not have effective boundary condition at infinity. Another concern is that the magnetic field decays only slowly at infinity, as $B \sim \exp(\pm i\alpha r)/r$, like a spherical wave. The magnetic energy, therefore, diverges generally.

The next difficulty is related to the uniqueness of the solution. The uniqueness is guaranteed if the homogeneous equation

$$(\Delta + \lambda^2)P = 0, \qquad B_n = 0 \quad (z = 0), \tag{5.5}$$

only has the trivial solution $\mathbf{B} = 0$. On the other hand Equation (5.5) has eigensolutions when λ's take particular values (eigenvalues), denoted here by $\lambda_0, \lambda_1, \lambda_2, \ldots$. Therefore, if α in Equation (5.3) coincides with one of λ's, the solution is not unique because one can add the eigensolution of arbitrary magnitude to the solution.

Before getting into a detailed discussion on the uniqueness of the solution, we will first summarize the methods of solution in the following. As in the current-free case, we have both Green's function approach and Fourier method.

5.3. Fourier expansion method

In the Fourier method (Nakagawa and Raadu, 1972), P is expanded as

$$P = \sum_{\mathbf{k}_\perp} P_{\mathbf{k}_\perp} \exp(i\mathbf{k}_\perp \cdot \mathbf{x}_\perp - Kz) \quad (K = \sqrt{k_\perp^2 - \alpha^2}). \tag{5.6}$$

This form satisfies Equation (5.3). As in the case of the current-free field, the summation $\sum$ excludes $\mathbf{k}_\perp = 0$. For the moment we assume that all the $\mathbf{k}_\perp$'s are restricted to the domain $k_\perp^2 > \alpha^2$ so that K is real. The Fourier coefficient $P_{\mathbf{k}_\perp}$ is related to $B_{\mathbf{k}_\perp}$ of Equation (4.8) by

$$P_{\mathbf{k}_\perp} = k_\perp^2 B_{\mathbf{k}_\perp} \quad (\mathbf{k}_\perp \neq 0). \tag{5.7}$$

The three components of the magnetic field are given as

$$B_x = \sum_{\mathbf{k}_\perp} (+i) B_{\mathbf{k}_\perp} k_\perp^{-2} (\alpha k_y - k_x K) \exp(i\mathbf{k}_\perp \cdot \mathbf{x}_\perp - Kz), \tag{5.8}$$

$$B_y = \sum_{\mathbf{k}_\perp} (-i) B_{\mathbf{k}_\perp} k_\perp^{-2} (\alpha k_x + k_y K) \exp(i\mathbf{k}_\perp \cdot \mathbf{x}_\perp - Kz), \tag{5.9}$$

$$B_z = \sum_{\mathbf{k}_\perp} B_{\mathbf{k}_\perp} \exp(i\mathbf{k}_\perp \cdot \mathbf{x}_\perp - Kz). \tag{5.10}$$

When $\alpha = 0$, these formulae reduce to those of the current-free field, Equations (4.10) – (4.12), except that the *DC* component B_{n0} must vanish. Seehafer (1978) devised a scheme which is free from this restriction.

In order to discuss the uniqueness of the solution, we consider the domain of computation as $0 \leqq x \leqq L_x$, $0 \leqq y \leqq L_y$, and $0 \leqq z \leqq L_z$. Equations (5.8)–(5.10) correspond to the case of $L_z = \infty$. We consider the eigensolutions which are periodic in x and y. The eigenvalues λ are expressed as

$$\lambda^2 = (2\pi n_x/L_x)^2 + (2\pi n_y/L_y)^2 + (\pi n_z/L_z)^2, \tag{5.11}$$

where n_x, n_y, and n_z are integers and at least one of them must be non-zero. If the value of α does not coincide with any of λ's, the solution is unique. This may happen, for example, if α^2 is smaller than the smallest λ^2, namely $|\alpha| < \min(2\pi/L_x, 2\pi/L_y, \pi/L_z)$. As long as L_x, L_y, and L_z are finite, the eigenvalues are discrete. Therefore, α generally falls between the eigenvalues and the uniqueness holds. If $L_z = \infty$ on the contrary, the eigenvalues densely fill the interval $|\lambda| \geqq \lambda_{\min} = \min(2\pi/L_x, 2\pi/L_y)$. If α is large such that $|\alpha| \geqq \lambda_{\min}$, the solution is not unique.

If $|\alpha| \geqq \lambda_{\min}$, some $\mathbf{k}_\perp$'s violate the condition $k_\perp^2 > \alpha^2$. Equations (5.8)–(5.10) no longer hold consequently. The quantity K in these equations becomes imaginary, and the z-dependence of the solutions is not exponential but sinusoidal. This feature reflects the appearance of eigensolutions. The eigensolutions have infinite magnetic energy (Berger, 1985).

One may be happy as long as α is small ($|\alpha| < \lambda_{\min}$), or if the given data have no Fourier components in the wavenumber range $k_\perp^2 < \alpha^2$. But suppose we are studying an isolated active region which happens to be the only active region on the solar visible surface. Then a natural choice would be to set $L_x \sim L_y \sim$ solar diameter. Then the allowable value for α is small and the deviation from the current-free field would hardly be visible within the active region. One may choose L_x and L_y such that the computational area is just as large as the active region. One may then assign a relatively large value for α. The latter approach however looks rather *ad hoc*.

5.4. Green's function method

Chiu and Hilton (1977) derived the Green's function for the constant-α force-free field. The poloidal scalar P is expressed as

$$P = \int B_n(\mathbf{x}') G_\alpha(\mathbf{x}, \mathbf{x}') \, dx' \, dy'. \tag{5.12}$$

In the local cylindrical coordinate system $\mathbf{x} - \mathbf{x}' = (R, \varphi, z)$, the Green's function G_α is written as

$$G_\alpha = \mathrm{Re}\frac{1}{2\pi}\int_0^\infty J_0(kR)\exp[-z(k^2-\alpha^2)^{1/2}]\,\mathrm{d}k/k\,, \tag{5.13}$$

where J's are Bessel functions, and Re means taking a real part. Equation (5.13) satisfies the Helmholtz equation (5.3). The components of the magnetic field are more conveniently expressed in terms of an auxiliary function $\Gamma = \partial G_\alpha/\partial R$,

$$\begin{aligned}\Gamma &= -\mathrm{Re}\frac{1}{2\pi}\int_0^\infty J_1(kR)\exp[-z(k^2-\alpha^2)^{1/2}]\,\mathrm{d}k = \\ &= \mathrm{Re}\frac{1}{2\pi}\frac{R}{z}\left[\frac{\exp(-ikr)}{r} - \frac{\exp(-ikz)}{z}\right],\end{aligned} \tag{5.14}$$

with $r = \sqrt{R^2+z^2}$. The Cartesian components of the magnetic field vector are

$$\mathbf{B}(\mathbf{x}) = \int B_n(\mathbf{x}')\begin{pmatrix}\partial\Gamma/\partial z(x-x')/R + \alpha\Gamma(y-y')/R \\ \partial\Gamma/\partial z(y-y')/R - \alpha\Gamma(x-x')/R \\ -\partial\Gamma/\partial R - \Gamma/R\end{pmatrix}\mathrm{d}x'\,\mathrm{d}y'\,. \tag{5.15}$$

The wavenumber spectrum of G_α or Γ consist of both $\exp(-z\sqrt{k^2-\alpha^2})$ (for $k^2 > \alpha^2$) and $\sin(z\sqrt{\alpha^2-k^2})$ (for $k^2 < \alpha^2$) terms. The latter contribution makes the energy divergent at infinity. If we replace Re with Im (imaginary part) in Equations (5.13)–(5.14), the resulting magnetic field satisfies the homogeneous boundary condition $B_n = 0$. Therefore, we may add such homogeneous solutions to Equation (5.15). The wavenumber spectrum of homogeneous solutions consist of $\cos(z\sqrt{\alpha^2-k^2})$ terms ($k^2 < \alpha^2$). Their energy is divergent.

5.5 Uniqueness of Solution

The uniqueness of constant-α solutions is guaranteed if $|\alpha|$ is smaller than the smallest eigenvalue of Equation (5.5). When the volume of consideration extends to infinity, the smallest eigenvalue is arbitrarily close to 0, so that the only unique solution is the current-free field. One may generally be forced to adopt a finite volume because of computational restrictions, but one needs a physical justification for doing so.

The recent knowledge (Taylor, 1986) that the helicity will be conserved even in the presence of magnetic diffusion (reconnection) could be a justification. The magnetic reconnection rapidly releases the energy and homogenizes the local helicities. Therefore, α becomes constant within a volume in which the reconnection process has propagated. The extent of such a volume will depend on the initial magnetic configuration and on a subsequent development of instabilities that facilitate the reconnection. In a laboratory plasma one may take the whole volume inside the apparatus and can apply constant-α

force-free modeling to it. In the case of the Sun no such enclosures exist. One should also notice that the model in which α is a constant in some volume and $\alpha = 0$ elsewhere cannot be treated in the framework of the constant-α modeling. Due to the restriction that α is constant along the field line (Equation (1.5)), the boundary between different values of α must be a magnetic flux surface which is however unknown until the problem is solved.

Hannakam *et al.* (1984) argued that the constant-α force-free fields can be uniquely determined by specifying the horizontal components of the magnetic field on the boundary. This argument is based on the uniqueness theorem described by Stratton (1941). Both arguments are incorrect. If one specifies $\mathbf{B}_h$ on the boundary, B_n is also fixed because of Equation (1.6). The specification of all the three components on the boundary overdetermines the problem and no solutions exist generally.

6. General Force-Free Fields

6.1. Variational principle

We will use the Euler potential expression (3.3) for **B**. The values of (f, g) are fixed on the boundary. We are, therefore, considering a family of magnetic fields which all share the same connectivity of field lines. The variation of energy W is

$$4\pi\delta W = \int (\delta f \nabla g - \delta g \nabla f) \cdot \operatorname{curl} \mathbf{B}\, \mathrm{d}V + \int \{\mathrm{d}\mathbf{S} \times (\delta f \nabla g - \delta g \nabla f)\} \cdot \mathbf{B}\,. \tag{6.1}$$

The extremum is described by

$$\nabla f \cdot \operatorname{curl} \mathbf{B} = \nabla g \cdot \operatorname{curl} \mathbf{B} = 0\,, \tag{6.2}$$

which means

$$\operatorname{curl} \mathbf{B} \times \mathbf{B} = (\nabla g \cdot \operatorname{curl} \mathbf{B}) \nabla f - (\nabla f \cdot \operatorname{curl} \mathbf{B}) \nabla g = 0\,. \tag{6.3}$$

Therefore, general force-free fields are characterized as the extremum of energy when the connectivity of field lines is specified. The extremum is actually the minimum until the first unstable mode appears in the force-free field under consideration.

6.2. Characteristic surfaces

Equation (6.2) is a quasi-linear second-order partial differential equation for two unknowns (f, g). The characteristic surfaces, whose normal vector is ξ, are obtained by replacing $\nabla \to \xi$ in the second-order derivatives in Equation (6.2). The resulting homogeneous equations for ξ have non-vanishing solutions when their determinant $[= \xi^2 (\xi \cdot \mathbf{B})^2]$ is zero. Of four characteristic surfaces, two of them are imaginary and the other two coincide with the magnetic surface. The latter condition reflects the fact that the magnetic field may have discontinuities (current sheets). The discontinuities appear as $\operatorname{curl} \mathbf{B} \to \infty$ and $\mathbf{B} \to 0$, so that the force-free equation (1.2) remains satisfied there

(formally). On the contrary Equations (3.6) and (5.3) are elliptic and no discontinuities appear in the solution. One may create a discontinuous solution by 'cutting and pasting' the two solutions, but Equation (3.6) or (5.3) is not satisfied at the discontinuity.

6.3. Direct minimization of energy with given connectivity

Since Equation (6.2) is nonlinear, no standard techniques are available to obtain the solution. One approach based on the variational principle given above was taken by Sakurai (1979). (See also Zwingmann (1987) for two-dimensional cases.) If one assumes some functions for the Euler potentials (f, g), one can evaluate the magnetic energy. (The magnetic energy is a functional of f and g.) Since the solution is characterized by the minimum of the energy, the functions (f, g) should be so selected that the energy is as small as possible. In order to carry out the minimum search in a systematic way, the trial functions (f, g) may include several adjustable parameters. The magnetic energy is now a function of these adjustable parameters, and standard techniques for function minimization are applicable.

It is advantageous to introduce a curvilinear coordinate system (f, g, s) where s is the arc-length along the field line. Then we can rewrite the functions $f(\mathbf{x}), g(\mathbf{x}), s(\mathbf{x})$ inverted as $\mathbf{x} = \mathbf{x}(f, g, s)$. The trial functions $\mathbf{x}(f, g, s)$ then specify the shape $\mathbf{x}(s)$ of the field line labeled as (f, g). This is analogous to the change in representation from Eulerian to Lagrangian, where (f, g, s) are the material coordinates.

As to the boundary condition, $\mathbf{x}(f, g, s)$ must be fixed on the boundary. The footpoints of field lines are moved together with the fluid, and the boundary condition correctly reflects this situation. When one deals with the geometry of flux tubes such as coronal loops, the end boundaries (cross-sectional boundaries) are subject to such boundary condition. On the lateral boundary, however, the specification of the shape of the boundary surface seems too restrictive. The boundary condition can be changed to a more natural pressure-balanced free boundary by properly modifying the expression for the energy to be minimized (Sakurai, 1979).

Figure 6 is an example. The initial current-free state (a) evolves into a force-free field (b) when the motion on the boundary $z = 0$ twists up the tube. The lateral boundary is supported by an external pressure.

6.4. Solution by specifying the distribution of α

The approach explained in the previous section is most suitable for studying the evolution of magnetic field structures due to the motion on the boundary. From the standpoint of realistic application, however, the boundary condition required in this approach, namely the connectivity of field lines, is not what can easily be derived from observations.

Another approach which makes use of the magnetic vector observations was introduced by Sakurai (1981). When the magnetic field vectors on the photosphere are measured, one can derive the distribution of α by

$$\alpha = \left(\frac{\partial B_y}{\partial x} - \frac{\partial B_x}{\partial y} \right)_{z=0} B_n^{-1} . \tag{6.4}$$

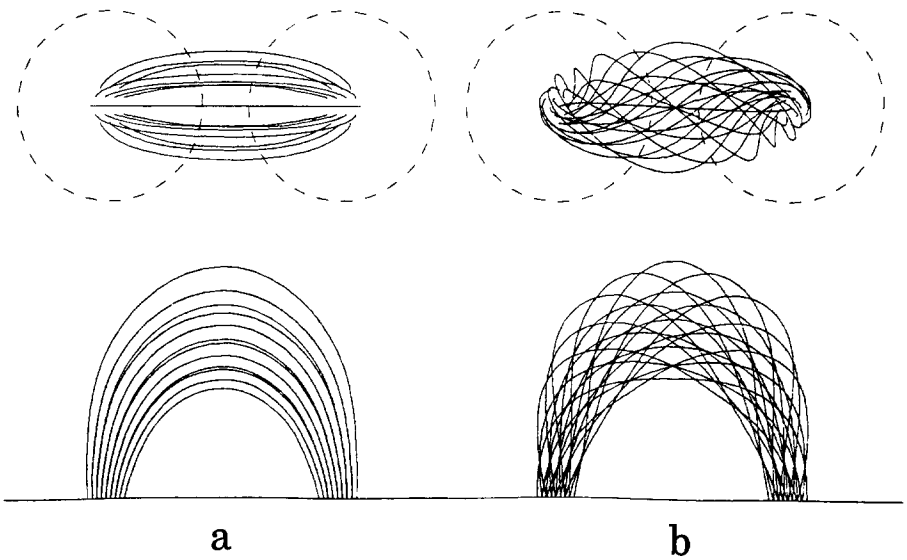

Fig. 6. Current-free (a) and force-free (b) magnetic fields calculated by the method of Section 6.3: top view (*top*) and side view (*bottom*). The motion applied on the boundary is such as to twist the tube (from Sakurai, 1979).

The value of α should be constant along the field line, but the shape of field lines is not available until the solution is found. Therefore, if α is specified on the whole $z = 0$ plane, this will generally lead to a conflict. As a matter of fact only the value of α either in the positive or in the negative flux region is enough in determining the force-free field solution. (B_n should be specified on the whole z-plane.)

The magnetic field $\mathbf{B}$ is written as

$$\mathbf{B} = \mathbf{B}_0 + \mathbf{B}_c\,, \tag{6.5}$$

where $\mathbf{B}_0$ is the current-free field corresponding to the boundary value B_n. The field $\mathbf{B}_c$ is due to the electric current and is written by Biot–Savart law as

$$\mathbf{B}_c = \operatorname{curl} \mathbf{A}_c\,, \tag{6.6}$$

$$\mathbf{A}_c(\mathbf{x}) = \frac{1}{c}\int \frac{\mathbf{j}(\mathbf{x}')}{|\mathbf{x} - \mathbf{x}'|}\,\mathrm{d}V'\,. \tag{6.7}$$

The integration with respect to $\mathbf{x}'$ is carried out both in $z > 0$ and in $z < 0$. The current $\mathbf{j}$ in the volume $z < 0$ is defined by a mirror symmetry,

$$\left.\begin{aligned} j_x(x, y, -z) &= -j_x(x, y, z) \\ j_y(x, y, -z) &= -j_y(x, y, z) \\ j_z(x, y, -z) &= +j_z(x, y, z) \end{aligned}\right\} (z > 0)\,. \tag{6.8}$$

This leads to $\mathbf{A}_c$ which is perpendicular to the $z = 0$ plane, so that $\mathbf{B}_c$ has vanishing normal component at $z = 0$.

The electric current **j** on the other hand should satisfy

$$\mathbf{j} = \frac{c\alpha}{4\pi}\mathbf{B}, \tag{6.9}$$

for the field **B** to be force-free. If we give an arbitrary **B**, define **j** by Equation (6.9), and re-calculate **B** by Equations (6.5)–(6.7), the last **B** is generally different from the first **B**. The force-free field solution can be found by making the two **B**'s consistent, by using an iterative procedure. The solution certainly exists when $\alpha = 0$ (the current-free field). As long as α is small, the existence of solution is guaranteed (Bineau, 1972), and the solution will be dynamically stable (Molodensky, 1976).

It is to be stressed here that not all the vector components of **B** are necessary in carrying out the procedure described above. The horizontal magnetic field $\mathbf{B}_h$ can be decomposed into a solenoidal (divergence-free) part and an irrotational (curl-free) part. The procedure given above only utilizes B_n on the whole z-plane and the solenoidal part of $\mathbf{B}_h$ in the region of certain (positive or negative) polarity. The computed force-free field will reproduce these components but not necessarily the other components.

Figure 7 shows an example of calculation. First a current-free configuration (a) is calculated, and a volume threaded by several field lines is picked up in order to assign a non-zero value of α. The resulting force-free field (b) shows twisted field lines due to the current flowing in the loop. Dashed lines are in the volume where no currents are assigned, but they also are disturbed by the current flowing in the loop.

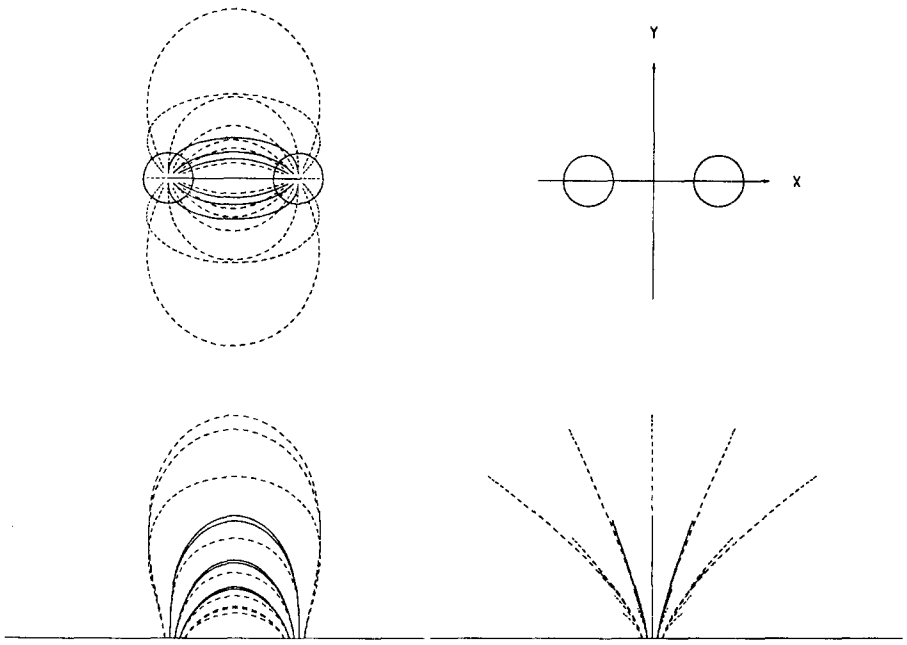

a

Fig. 7a.

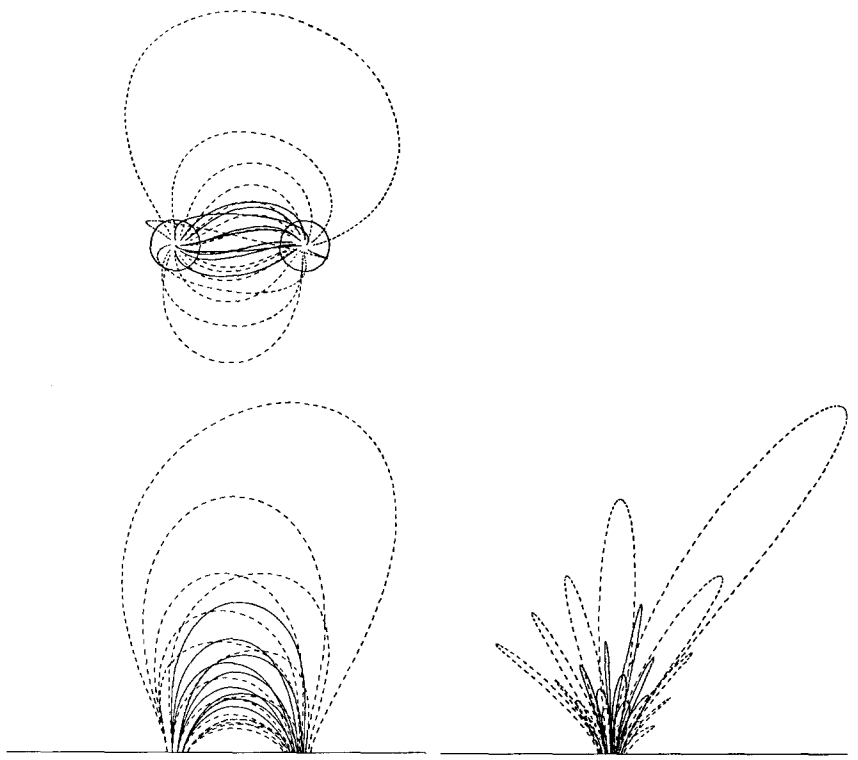

Fig. 7. Current-free (a) and force-free (b) magnetic fields calculated by the method of Section 6.4. The distribution of α in Figure 7(b) is like a step function, namely α = constant > 0 in the tubular volume threaded by solid field lines, and $\alpha = 0$ elsewhere (from Sakurai, 1981).

6.5. Pridmore-Brown's method

Pridmore-Brown (1981) attacked the problem by means of the so-called Method of Weighted Residuals (e.g., Finlayson, 1972). The magnetic field is decomposed into the current-free component $\mathbf{B}_0$ and the current-associated component $\mathbf{B}_c$ as in Equation (6.5). The $\mathbf{B}_0$-component is represented by the Fourier series as in Section 4.4, and is uniquely determined by specifying B_n. The $\mathbf{B}_c$-component is also Fourier expanded in such a form that it gives vanishing normal component on the z-plane. The unknown Fourier coefficients in the $\mathbf{B}_c$-component is determined by minimizing the sum of the square of the following quantities:

(i) the volume integral of Lorentz force, and

(ii) the difference between the observed and calculated directions of the horizontal magnetic field.

In (ii), the observed direction of the horizontal magnetic field is supposed to be given by the direction of fibrils in the Hα photographs. Therefore the boundary conditions used in this method are the values of B_n and B_x/B_y over the z-plane. Mathematical proof is not available which guarantees the existence of the solution in this approach.

The method of Section 6.4 is based on the finite element representation of the current flow. The finite element approach is most appropriate if the electric current is limited within a small volume. The Fourier method is less effective in such a case because it has to handle the whole volume anyway. As the current distribution becomes diffuse, the Fourier expansion becomes at least equally effective as the finite element method. In some cases the finite element approach introduces a complicated handling of the elements, and becomes less effective than the simple Fourier method.

6.6. Integration in z as an initial value problem

Nakagawa (1974) and Wu *et al.* (1985) tried to solve the force-free equation by direct integration of this equation via finite differencing,

$$\frac{\partial B_x}{\partial z} = \alpha B_y + \frac{\partial B_z}{\partial x} , \tag{6.10}$$

$$\frac{\partial B_y}{\partial z} = -\alpha B_x + \frac{\partial B_z}{\partial y} , \tag{6.11}$$

$$\frac{\partial B_z}{\partial z} = -\frac{\partial B_x}{\partial x} - \frac{\partial B_y}{\partial y} , \tag{6.12}$$

$$\frac{\partial \alpha}{\partial z} = \left(B_x \frac{\partial \alpha}{\partial x} + B_y \frac{\partial \alpha}{\partial y} \right) B_z^{-1} . \tag{6.13}$$

The boundary condition requires the magnetic vector **B** at $z = 0$.

When the boundary condition is such that $\alpha = 0$ on the z-plane, this method leads to the Cauchy integration of the Laplace equation. In the Cauchy problem of the Laplace equation, the Laplace equation is integrated as an initial value problem in which z is the time variable and the value of **B** is given at $z = 0$ as the initial condition. As is well known, this is an ill-posed problem and the integration diverges. The reason is that the Laplace equation, when integrated with respect to z, has both exponentially decaying and growing solutions. Even if the initial condition only contains the decaying solutions, the growing solutions sneak in due to numerical errors.

This undesirable situation will appear in the force-free field equation as well. Wu *et al.* (1985) applied their method to a known analytic force-free field model and confirmed the accuracy in their procedure. This, however, does not guarantee the success of their method in realistic cases. An irregular distribution of magnetic fields in realistic data will be a source of larger numerical errors. It should also be remembered that, in the ill-posed problems, the reduction in the grid size will not lead to the increase in the accuracy but to the earlier breakdown in the integration.

6.7. Frictional methods

Yang *et al.* (1986) and Craig and Sneyd (1986) modified the force-free equation into a time-dependent equation with a frictional term which is proportional to the Lorentz

force. Starting from an initial non-equilibrium state, the system relaxes under the frictional drag. In the final state the system is at rest without friction (i.e., the Lorentz force in balance), and the force-free equilibrium is obtained.

Yang *et al.* (1986) modified Equation (6.2) into

$$\frac{\partial f}{\partial t} = -\nu^{-1}\mathbf{F}_B \cdot \nabla f, \qquad \frac{\partial g}{\partial t} = -\nu^{-1}\mathbf{F}_B \cdot \nabla g, \tag{6.14}$$

where $\mathbf{F}_B$ is the Lorentz force and ν is a fictitious coefficient of friction. Craig and Sneyd (1986) make use of the Lagrangian description of the fluid and write

$$\frac{\mathrm{D}\mathbf{x}}{\mathrm{D}t} = \nu\mathbf{F}_B . \tag{6.15}$$

Here $\mathbf{x}(\mathbf{X}, t)$ is the location at time t of the fluid element which was initially situated at $\mathbf{X}$. The Lagrangian time derivative $\mathrm{D}/\mathrm{D}t$ is taken for a fixed $\mathbf{X}$. These two approaches are essentially the same because the Euler potentials are regarded as the two Lagrangian coordinates in the direction transverse to the magnetic field. On the boundary, the values of (f, g) or $\mathbf{x}$ are specified.

7. Applications

7.1. 'Vectorization' of vector magnetograms

As was described in Section 2, measurements by vector magnetographs give two possible vectors for transverse fields, either $\mathbf{B}_t$ or $-\mathbf{B}_t$. Several methods have been proposed to resolve this ambiguity in the azimuth of the transverse field. Krall *et al.* (1982) selected the vector which is closer to the local gradient of the longitudinal field $(-\nabla B_l)$, because generally the field runs from positive to negative polarities. Sakurai *et al.* (1985) calculated the current-free field based on the observed B_l, and assigned the direction of $\mathbf{B}_t$ in referring to the current-free field vector (Figure 8, *left*). Both methods may have a conservative bias, leading to less distorted magnetic field.

Once the field vector $(\mathbf{B}_t, B_l)$ for the observer is determined, we may express it in the solar frame as $(\mathbf{B}_h, B_n)$ according to the location of the observed region on the Sun. This process, however, mixes B_l with less accurate $\mathbf{B}_t$. As long as the region of interest is not very far from the disk center, it would be advisable to simply set $\mathbf{B}_h = \mathbf{B}_t$ and $B_n = B_l$.

An example of application obtained from this vectorization is that we can then calculate the vertical gradient of the magnetic field in sunspots by

$$\left.\frac{\partial B_z}{\partial z}\right|_{z=0} = -\nabla_h \cdot \mathbf{B}_h . \tag{7.1}$$

This quantity has also been derived by measuring the longitudinal magnetic fields in two spectral lines which are formed in different heights in the solar atmosphere (Makita and

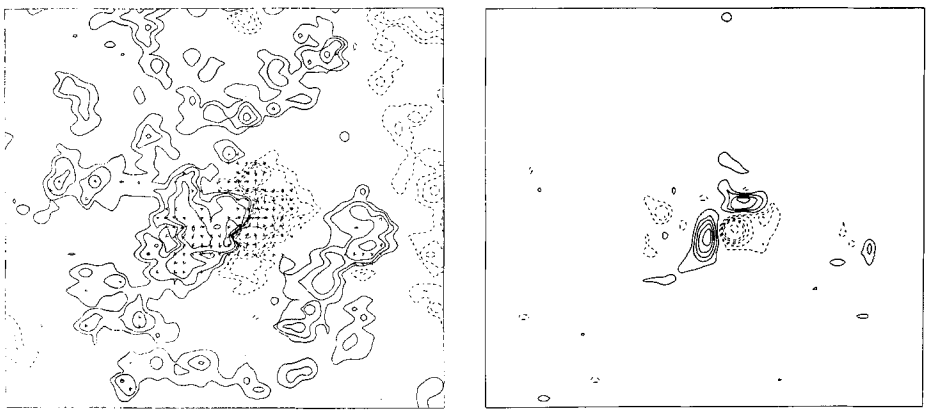

Fig. 8. Magnetic field vector (*left*) and electric current distribution (*right*) in the active region NOAA 4187 (May 26, 1983) observed by the vector magnetograph of Okayama Station, National Astronomical Observatory of Japan. Positive and negative longitudinal fields are represented by solid and dotted contours, respectively, with levels ± 10, 20, 50, 100, 200, and 500 G. Arrows indicate the transverse field vector. The electric currents are here shown in terms of curl $\mathbf{B}_t$, with contour levels ± 20, 40, 60, 80, and 100 G/10^4 km (from Sakurai *et al.*, 1985).

Nemoto, 1976, and references cited therein). A comparison between the two methods is found in Hagyard *et al.* (1985).

When the observed transverse field deviates significantly from the computed current-free field, it indicates the existence of electric currents. Such magnetic configuration is called to have a large shear, and is closely related to the flare activity (Hagyard *et al.*, 1984; Patty and Hagyard, 1986; Hofmann *et al.*, 1987). This point can be addressed more directly in terms of the electric current distribution derived from magnetic vector observations.

7.2. Electric Current Distribution

We can derive the normal component of electric current density from observations by

$$j_n = \frac{c}{4\pi} \mathbf{n} \cdot \operatorname{curl} \mathbf{B}_h \,. \tag{7.2}$$

An example is shown in Figure 8 (*right*). The association between flare knots and regions of large j_n was originally pointed out by Moreton and Severny (1968), and was extensively studied in the Solar Maximum Mission era (Krall *et al.*, 1982; Lin and Gaizaukas, 1987; Ding *et al.*, 1987; a review by Hagyard *et al.*, 1986). The relation between j_n and bright points seen in the *XUV* wavelengths was studied by de Loach *et al.* (1984) and by Haisch *et al.* (1986). Kotov (1971) derived the electric current vector **j** from the magnetic vectors $\mathbf{B}(z_1)$ and $\mathbf{B}(z_2)$ by using two spectral lines that correspond to different heights (z_1 and z_2) in the atmosphere.

If the force-free field approximation is valid, the value of α is obtained by

$$\alpha = (4\pi/c) j_n / B_n \,. \tag{7.3}$$

Sakurai *et al.* (1985) calculated the force-free field by using the distribution of α thus obtained, by applying the method described in Section 6.4 (Figure 9).

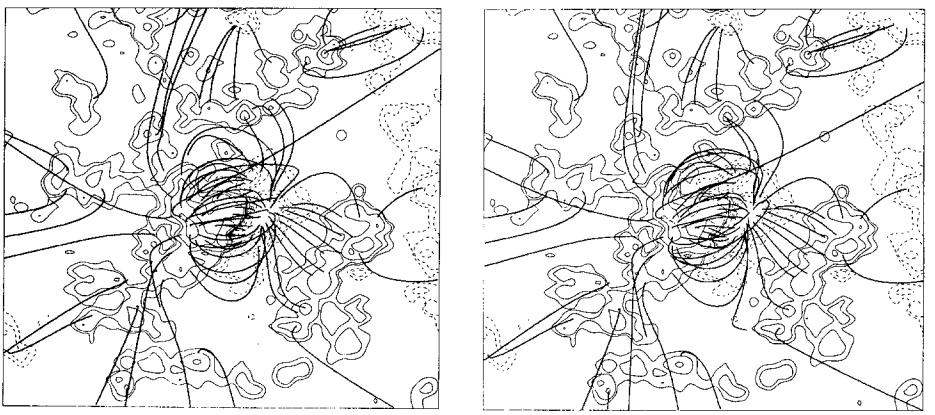

Fig. 9. Current-free (*left*) and force-free (*right*) magnetic fields calculated from the magnetic data of Figure 8. Field lines in the two figures have the same footpoints, so that the difference between the two is due to the effects of the electric currents (from Sakurai *et al.* 1985).

Sometimes one encounters a conflicting situation, however. For example a large value of j_n is found on the magnetic neutral line where $B_n = 0$. Global force-balance relations described in Section 3.3, which must hold for force-free fields, were examined by Gary *et al.* (1987) and were found to be satisfied. Sakurai (1987), however, found a large deviation in several active regions.

Since there is no reason to believe that the force-free assumption applies down to the photospheric level where the magnetic field is observed, the validity of Equation (7.3) should be considered critically. For this purpose we divide the electric currents into two categories, namely the force-free (field-aligned) currents and the non-force-free currents. The former currents have the scale length as large as that of the magnetic field itself. The latter currents are caused by non-magnetic forces in the photosphere and will be confined within a thin layer of thickness h. The magnitude of h will be a few times the photospheric scale height, for example $h = 500$ km. We designate by $\mathbf{B}$ the observed field vector at $z = 0$ (photosphere) as before, and by $\mathbf{B}'$ the field vector at $z = h$. The normal component of the electric current j_n at $z = 0$ is derived by Equation (7.2).

Now we will apply the method described in Section 6.4 to the volume $z > h$. We then need the boundary values B_n' and j_n'. The approximation $B_n' = B_n$ will be justified because h is small compared with the lateral characteristic length scale of the field. For the electric current we set $j_n' = j_n$ as the first guess. The force-free field solution gives the value of $\mathbf{B}'$, from which we can calculate the surface electric current $\mathbf{J}_h = (J_x, J_y)$ integrated over the range $0 < z < h$,

$$J_x = -\frac{c}{4\pi}(B_y' - B_y), \tag{7.4}$$

$$J_y = +\frac{c}{4\pi}(B'_x - B_x)\,. \tag{7.5}$$

If we require that the force vector $\mathbf{J}_h \times \mathbf{B}$ should lie in the horizontal plane, we obtain the condition,

$$B'^2_h = B^2_h\,. \tag{7.6}$$

The first guess will not generally fulfill this condition. We may then deviate from the initial guess $j'_n = j_n$ so that Equation (7.6) is satisfied. This scheme is however much more complicated than the original method.

7.3. Magnetic Energy Storage

The total amount of energy stored in the volume $z > 0$ can be calculated in various ways. For the current-free field, the energy is represented as

$$W_0 = \frac{1}{8\pi}\int_{z=0} \phi B_n \,\mathrm{d}x\,\mathrm{d}y\,. \tag{7.7}$$

In the Fourier expansion methods for constant-α force-free fields (including the current-free field), the energy is written as

$$W = \sum |B_{\mathbf{k}_\perp}|^2 \frac{L_x L_y}{K}\,. \tag{7.8}$$

For the general force-free fields, the energy W is the quantity to be minimized in the method of Section 6.3 so that it is readily available. In the method of Section 6.4, the energy is evaluated by

$$W = \frac{1}{2c}\int_{z>0} \mathbf{A}_c \cdot \mathbf{j}\,\mathrm{d}V + W_0\,. \tag{7.9}$$

One may also utilize the virial relation (3.20).

The energy of the current-free field W_0 is associated with the currents flowing under the photosphere. Therefore, in rapid processes like flares, W_0 will not change and can be regarded as the constant base level of the energy. If any changes in magnetic energy are to take place during the flare, those will be associated with the currents flowing in the chromosphere/corona. The amount of energy that can be liberated is $W - W_0$, which might be called the magnetic free energy stored in the atmosphere.

By applying a simple constant-α force-free field model, Tanaka and Nakagawa (1973) obtained that $W - W_0$ was of the order of 10^{32} ergs in the active region of August 1972 which produced several large flares. A more detailed treatment by Seehafer and Staude (1979) gave a similar value. Since the constant-α model could not reproduce the magnetic field structure precisely, it would be premature to say that the flare energy build-up was detected in a quantitative sense.

Gary *et al.* (1987) applied the virial relation (3.20) to estimate the energy stored in an active egion of September 1980. They found that $W - W_0$ is of the order of 10^{32} ergs. Sakurai (1987) applied the same technique to many active regions and found that $W - W_0$ shows a large scatter, even $W - W_0 < 0$ in some regions. This might mean the breakdown of force-free assumption in some active regions.

7.4. Computed field lines and magnetic tracers

The most common way of representing the structure of the magnetic field is to draw field lines. When $\mathbf{B}(\mathbf{x})$ is available by the methods described in Sections 4–6, the magnetic field lines are obtained by integrating

$$\frac{d\mathbf{x}}{ds} = \frac{\mathbf{B}(\mathbf{x})}{|\mathbf{B}(\mathbf{x})|} , \tag{7.10}$$

where s is the arc-length along the field line. The starting points of the field lines are usually distributed in such a way that the density of the footpoints of the field lines is proportional to B_n (or magnetic flux).

If the field lines pass through the region near magnetic neutral points, their trajectory is very sensitive to the selection of the starting points. In order not to be deceived by such untypical field lines, one should integrate enough number of field lines. Needless to say, field lines that do not exist in the solution will not appear, although one may miss the existing field lines.

Computed field lines were compared with thread-like structures on the Sun: chromospheric fibrils (Nakagawa *et al.*, 1971), post-flare loops (Rust and Roy, 1971), coronal X-ray loops (Poletto *et al.*, 1975; Sakurai and Uchida, 1977), and so on. The underlying expectation is that these structures form along the magnetic field. This expectation has been vindicated in a broad sense. If we appreciate that the alignment of these features along the magnetic field is so fundamental as not to fail, we may reverse the argument. We may check the validity of, or constrain the ambiguity in, the computational models for the magnetic field.

One of such approaches has been made when one tries to determine the value of α in the constant-α force-free field model. Frequently a single value of α is found to be insufficient in reproducing the observed structures. Levine (1976), for example, argued that different X-ray loops in an active region have different values (signs) of α. Gary *et al.* (1987) obtained the sign of α point by point in an active region, by comparing which sign of α better reproduces the magnetic tracers. These treatments are however inconsistent with the assumption of α = constant, and no much weight can be attached.

8. Concluding Remarks

8.1. Computational methods when $\mathbf{l} \neq \mathbf{n}$

When the region to be studied is not close to the disk center, and $\mathbf{n}$ is significantly different from $\mathbf{l}$ (viz., oblique geometry), the applicability of methods described in

Sections 4–6 is as follows. For the current-free modeling, the Green's function method can be extended to the oblique geometry (Semel, 1967) and to the spherical geometry as well (Sakurai, 1982). The uniqueness in the solution in these cases was discussed by Aly (1987). The Fourier method (Wellck and Nakagawa, 1973) can handle the oblique geometry for the constant-α force-free field (which includes the current-free case). The Green's function of Chiu and Hilton (1977) has not been modified to the oblique cases.

Various methods for general force-free fields are developed for the cases with $\mathbf{n} = \mathbf{l}$. Since some of these methods are meaningful only when the magnetic field vector is available as the boundary condition, one may always derive $(\mathbf{B}_h, B_n)$ from $(\mathbf{B}_t, B_l)$. In this sense the oblique geometry can be handled. As was discussed in the previous section, however, the derived B_n will be deteriorated by the relatively inaccurate $\mathbf{B}_t$. One should conservatively restrict the application of these methods to the head-on geometry $(\mathbf{n} = \mathbf{l})$.

8.2. Beyond the Force-Free Approximation

The inclusion of the effects of pressure and gravity has been made for idealized (two-dimensional) models (Low, 1982). The basic equation can be neatly written in terms of Euler potentials even in three-dimensional cases (Low, 1980). It is, therefore, possible to construct a realistic scheme for a fully magnetohydrostatic modeling. A more difficult problem is how to obtain the necessary boundary conditions from observations. Although full of difficulties, magnetic fields are constantly monitored by the magnetographs. On the other hand the temperature and the density at the photospheric level are largely uniform. The energy density carried by the plasma greatly exceeds the magnetic energy at the photosphere. Therefore a slight inhomogeneity in the temperature and/or density will have a great effect on the magnetic field.

Despite this difficulty, the deviation from the force-free state exists without doubt. Hα photographs show low-lying fibrils, indicative of the effect of gravity. Prominences will not form without gravity. A future direction would be to modify the force-free field modeling in a thin layer near the photosphere, where the deviation from the force-free equilibrium is most important.

8.3. Prospects

We have a difficulty in measuring the magnetic field on one hand, and a difficulty in computing the magnetic field model on the other hand. The latter difficulty is close to being resolved. The former, however, still stands. It may be that the situation is pessimistic, in that whatever we improve our instruments, the existence of inhomogeneous magnetic structures may prohibit us from obtaining the correct information on the solar magnetic fields.

The current view (Stenflo, 1976) is that the flux tubes are homogeneous in character and only their number density varies from position to position. If this is the case, the construction of 'standard flux tube' model would be of great help. The instruments like LEST (Andersen *et al.*, 1984) or HRSO (van Ballegooijen, 1985) are crucial in achieving this goal. On the other hand if the character of the flux tubes depends on the environ-

ment, one has to determine the flux tube parameters at the same time as the magnetic observations. This will require the upgrade of existing magnetographs. The Stokes (profile-recording) polarimeters as efficient as the usual magnetographs might be a solution. The nature of the activity of the Sun will ultimately be revealed when these difficulties are resolved.

In the coming activity maximum (1991–1992) of the 22-nd solar cycle, several coordinations in the flare research are being planned (FLARES 22 of COSPAR/SCOSTEP, MAX '91 of U.S.A.). As a joint Japan–U.S.A.–U.K. project, the SOLAR-A satellite with hard and soft X-ray imagers will be launched in 1991 (Ogawara, 1987). With the vector magnetograms and the coronal magnetic structures at hand, it is timely to pursue the computational modeling of magnetic fields. Methods described in Section 6 have to be tested on realistic data sets and should be ready by the advent of the activity maximum.

References

Adams, J. and Pneuman, G. W.: 1976, *Solar Phys.* **46**, 185.

Altschuler, M. D. and Newkirk, G., Jr.: 1969, *Solar Phys.* **9**, 131.

Altschuler, M. D., Levine, R. H., Stix, M., and Harvey, J. W.: 1977, *Solar Phys.* **51**, 345.

Aly, J. J.: 1987, *Solar Phys.* **111**, 287.

Andersen, T. E., Dunn, R. B., and Engvold, O.: 1984, *LEST Foundation Technical Report*, No. 7.

Antiochos, S. K.: 1987, *Astrophys. J.* **312**, 886.

Babcock, H. W.: 1953, *Astrophys. J.* **118**, 387.

Beckers, J. M.: 1971, in R. Howard (ed.), 'Solar Magnetic Fields', *IAU Symp.* **43**, 3.

Berger, M. A.: 1985, *Astrophys. J. Suppl.* **59**, 433.

Berger, M. A. and Field, G. B.: 1984, *J. Fluid Mech.* **147**, 133.

Bineau, M.: 1972, *Comm. Pure Appl. Math.* **25**, 77.

Birn, J. and Schindler, K.: 1981, in E. R. Priest (ed.), *Solar Flare Magnetohydrodynamics*, Gordon and Breach, London, p. 337.

Bray, R. J. and Loughhead, R. E.: 1979, *Sunspots*, Dover Publications, New York, p. 164.

Chandrasekhar, S.: 1960a, *Radiative Transfer*, Dover Publications, New York, p. 24.

Chandrasekhar, S.: 1960b, *J. Math. Anal. Appl.* **1**, 240.

Chiu, Y. T. and Hilton, H. H.: 1977, *Astrophys. J.* **212**, 873.

Cowling, T. G.: 1981, *Ann. Rev. Astron. Astrophys.* **19**, 115.

Craig, I. J. D. and Sneyd, A. D.: 1986, *Astrophys. J.* **311**, 451.

deLoach, A. C., Hagyard, M. J., Rabin, D., Moore, R. L., Smith, J. B., Jr., West, E. A., and Tandberg–Hanssen, E.: 1984, *Solar Phys.* **91**, 235.

Ding, Y. J., Hagyard, M. J., deLoach, A. C., Hong, Q. F., and Liu, X. P.: 1987, *Solar Phys.* **109**, 307.

Finlayson, B. A.: 1972, *The Method of Weighted Residuals and Variational Principles*, Academic Press, New York.

Gary, G. A., Moore, R. L., Hagyard, M. J., and Haisch, B. M.: 1987, *Astrophys. J.* **314**, 782.

Giovanelli, R. G.: 1980, *Solar Phys.* **68**, 49.

Hagyard, M. J.: 1985, *Measurements of Solar Vector Magnetic Fields*, NASA CP-2374.

Hagyard, M. J., Gaizauskas, V., Chapman, G. A., deLoach, A. C., Gary, G. A., Jones, H. P., Karpen, J. T., Martres, M.-J., Porter, J. G., Schmieder, B., Smith, J. B., Jr., and Toomre, J.: 1986, in M. Kundu and B. Woodgate (eds.), *Energetic Phenomena on the Sun*, NASA CP-2439, p. 1.

Hagyard, M. J., Teuber, D., West, E. A., Tandberg-Hanssen, E., and Henze, W., Jr.: 1985, in C. de Jager and Chen Biao (eds.), *Proceedings of Kumning Workshop on Solar Physics and Interplanetary Travelling Phenomena*, Science Press, Beijing, p. 204.

Hagyard, M. J., Smith, J. B., Jr., Teuber, D., and West, E. A.: 1984, *Solar Phys.* **91**, 115.

Haisch, B. M., Bruner, M. E., Hagyard, M. J., and Bonnet, R. M.: 1986, *Astrophys. J.* **300**, 428.

Hannakam, L., Gary, G. A., and Teuber, D. L.: 1984, *Solar Phys.* **94**, 219.
Harvey, J.: 1977, in E. A. Muller (ed.), *Highlights of Astronomy*, Vol. 4, IAU, p. 223.
Hofmann, A., Rendtel, J., Aurass, H., and Kalman, B.: 1987, *Solar Phys.* **108**, 151.
Kawakami, H.: 1983, *Publ. Astron. Soc. Japan* **35**, 459.
Kotov, V. A.: 1971, in R. Howard (ed.), 'Solar Magnetic Fields', *IAU Symp.* **43**, 212.
Krall, K. R., Smith, J. B., Jr., Hagyard, M. J., West, E. A., and Cumings, N. P.: 1982, *Solar Phys.* **79**, 59.
Kundu, M, R. and Woodgate, B.: 1986, *Energetic Phenomena on the Sun*, NASA CP-2439.
Kuperus, M., Ionson, J. A., and Spicer, D. S.: 1981, *Ann. Rev. Astron. Astrophys.* **19**, 7.
Landi Degl'Innocenti, E.: 1976, *Astron. Astrophys. Suppl.* **25**, 379.
Landi Degl'Innocenti, E.: 1979, *Solar Phys.* **63**, 237.
Leroy, J. L., Bommier, V., and Sahal-Brechot, S.: 1984, *Astron. Astrophys.* **131**, 33.
Levine, R. H.: 1976, *Solar Phys.* **46**, 159.
Levine, R. H., Schulz, M., and Frazier, E. N.: 1982, *Solar Phys.* **77**, 363.
Lin, Y. Z. and Gaizauskas, V.: 1987, *Solar Phys.* **109**, 81.
Low, B. C.: 1980, *Solar Phys.* **65**, 147.
Low, B. C.: 1982, *Rev. Geophys. Space Phys.* **20**, 145.
Low, B. C.: 1985, in M. J. Hagyard (ed.), *Measurements of Solar Vector Magnetic Fields*, NASA CP-2374, p. 49.
Makita, M.: 1979, *Publ. Astron. Soc. Japan* **31**, 575.
Makita, M. and Nemoto, K.: 1976, *Publ. Astron. Soc. Japan* **28**, 495.
Molodensky, M. M.: 1969, *Soviet Astron. AJ* **12**, 585.
Molodensky, M. M.: 1974, *Solar Phys.* **39**, 393.
Molodensky, M. M.: 1975, *Solar Phys.* **43**, 311.
Molodensky, M. M.: 1976, *Solar Phys.* **49**, 279.
Molodensky, M. M. and Syrovatsky, S. I.: 1977, *Soviet Astron.* **21**, 734.
Moreton, G. E. and Severny, A. B.: 1968, *Solar Phys.* **3**, 282.
Morse, P. M. and Feshbach, H.: 1953, *Methods in Theoretical Physics*, McGraw-Hill, New York, p. 1767.
Nakagawa, Y.: 1974, *Astrophys. J.* **190**, 437.
Nakagawa, Y. and Raadu, M. A.: 1972, *Solar Phys.* **25**, 127.
Nakagawa, Y., Raadu, M. A., Billings, D. E., and McNamara, D.: 1971, *Solar Phys.* **19**, 172.
Ogawara, Y.: 1987, *Solar Phys.* **113**, 361.
Parker, E. N.: 1979, *Cosmical Magnetic Fields*, Clarendon Press, Oxford, p. 207.
Patty, S. R. and Hagyard, M. J.: 1986, *Solar Phys.* **103**, 111.
Poletto, G., Vaiana, G. S., Zombeck, M. V., Krieger, A. S., and Timothy, A. F.: 1975, *Solar Phys.* **44**, 83.
Pridmore-Brown, D. C.: 1981, Aerospace Corporation Report ATR-81(7813)-1.
Riesebieter, W. and Neubauer, F. M.: 1979, *Solar Phys.* **63**, 127.
Rust, D. M. and Roy, J.-R.: 1971, in R. Howard (ed.), 'Solar Magnetic Fields', *IAU Symp.* **43**, 569.
Sakurai, T.: 1979, *Publ. Astron. Soc. Japan* **31**, 209.
Sakurai, T.: 1981, *Solar Phys.* **69**, 343.
Sakurai, T.: 1982, *Solar Phys.* **76**, 301.
Sakurai, T.: 1987, *Solar Phys.* **113**, 137.
Sakurai, T. and Uchida, Y.: 1977, *Solar Phys.* **52**, 397.
Sakurai, T., Makita, M., and Shibasaki, K.: 1985, in H. U. Schmidt (ed.), *Theoretical Problems in High Resolution Solar Physics*, MPA-212, Max-Planck-Institute, Munich, p. 312.
Schmidt, H. U.: 1964, in W. N. Hess (ed.), *NASA Symposium on the Physics of Solar Flares*, p. 107.
Seehafer, N.: 1978, *Solar Phys.* **58**, 215.
Seehafer, N. and Staude, J.: 1979, *Astron. Nachr.* **300**, 151.
Semel, M.: 1967, *Ann. Astrophys.* **30**, 513.
Stenflo, J. O.: 1971, in R. Howard (ed.), 'Solar Magnetic Fields', *IAU Symp.* **43**, 101.
Stenflo, J. O.: 1976, in V. Bumba and J. Kleczek (eds.), 'Basic Mechanisms of Solar Activity', *IAU Symp.* **71**, 69.
Stenflo, J. O.: 1978, *Rep. Prog. Phys.* **41**, 865.
Stern, D. P.: 1966, *Space Sci. Rev.* **6**, 147.
Stratton, J. A.: 1941, *Electromagnetic Theory*, McGraw-Hill, New York, p. 250.
Sturrock, P. A.: 1980, *Solar Flares*, Colorado Associated University Press, Boulder, Colorado.

Švestka, Z.: 1976, *Solar Flares*, D. Reidel Publ. Co., Dordrecht, Holland.
Tanaka, K. and Nakagawa, Y.: 1973, *Solar Phys.* **33**, 187.
Taylor, J. B.: 1986, *Rev. Mod. Phys.* **58**, 741.
Teuber, D., Tandberg-Hanssen, E., and Hagyard, M. J.; 1977, *Solar Phys.* **53**, 97.
Unno, W.: 1956, *Publ. Astron. Soc. Japan* **8**, 108.
van Ballegooijen, A.: 1985, Lockheed Palo Alto Research Laboratory Publication.
Wellck, R. E. and Nakagawa, Y.: 1973, *NCAR Technical Note,* NCARTN/STR-87.
West, E. A. and Hagyard, M. J.: 1983, *Solar Phys.* **88**, 51.
Woltjer, L.: 1958, *Proc. Nat. Acad. Sci.* **44**, 489.
Woltjer, L.: 1959, *Proc. Nat. Acad. Sci.* **45**, 769.
Wu, S. T., Chang, H. M., and Hagyard, M. J.: 1985, in M. J. Hagyard (ed.), *Measurements of Solar Vector Magnetic Fields*, NASA CP-2374, p. 17.
Yang, W. H., Sturrock, P. A., and Antiochos, S. K.: 1986, *Astrophys. J.* **309**, 383.
Zirin, H.: 1968, *Solar Phys.* **5**, 435.
Zwingmann, W.: 1987, *Solar Phys.* **111**, 309.